Proteasome-dependent protein quality control of the peroxisomal membrane protein Pxa1p

Devarajan, S.; Meurer, M.; van Roermund, C. W. T.; Chen, X.; Hettema, E. H.; Kemp, S.; Knop, M.; Williams, C.

Published in:
Biochimica et Biophysica Acta-Biomembranes

DOI:
10.1016/j.bbamem.2020.183342

Publication date:
2020

BBA - Biomembranes 1862 (2020) 183342

Contents lists available at ScienceDirect

BBA - Biomembranes

journal homepage: www.elsevier.com/locate/bbamem

Proteasome-dependent protein quality control of the peroxisomal membrane protein Pxa1p

S. Devarajan[a], M. Meurer[b], C.W.T. van Roermund[c], X. Chen[a], E.H. Hettema[d], S. Kemp[c], M. Knop[b,e], C. Williams[a,*]

[a] Department of Cell Biochemistry, University of Groningen, the Netherlands
[b] Zentrum für Molekulare Biologie der Universität Heidelberg (ZMBH), DKFZ-ZMBH Alliance, Heidelberg, Germany
[c] Laboratory Genetic Metabolic Diseases, Amsterdam University Medical Centres, the Netherlands
[d] Department of Molecular Biology, University of Sheffield, Sheffield, United Kingdom
[e] Cell Morphogenesis and Signal Transduction, German Cancer Research Centre (DKFZ), Heidelberg, Germany

ARTICLE INFO

Keywords:
Protein degradation
Proteasome
ALD
Peroxisome
ufd4

ABSTRACT

Peroxisomes are eukaryotic organelles that function in numerous metabolic pathways and defects in peroxisome function can cause serious developmental brain disorders such as adrenoleukodystrophy (ALD). Peroxisomal membrane proteins (PMPs) play a crucial role in regulating peroxisome function. Therefore, PMP homeostasis is vital for peroxisome function. Recently, we established that certain PMPs are degraded by the Ubiquitin Proteasome System yet little is known about how faulty/non-functional PMPs undergo quality control. Here we have investigated the degradation of Pxa1p, a fatty acid transporter in the yeast *Saccharomyces cerevisiae*. Pxa1p is a homologue of the human protein ALDP and mutations in ALDP result in the severe disorder ALD. By introducing two corresponding ALDP mutations into Pxa1p (Pxa1^{MUT}), fused to mGFP, we show that Pxa1^{MUT}-mGFP is rapidly degraded from peroxisomes in a proteasome-dependent manner, while wild type Pxa1-mGFP remains relatively stable. Furthermore, we identify a role for the ubiquitin ligase Ufd4p in Pxa1^{MUT}-mGFP degradation. Finally, we establish that inhibiting Pxa1^{MUT}-mGFP degradation results in a partial rescue of Pxa1p activity in cells. Together, our data demonstrate that faulty PMPs can undergo proteasome-dependent quality control. Furthermore, our observations may provide new insights into the role of ALDP degradation in ALD.

1. Introduction

Peroxisomes are eukaryotic organelles that encompass a protein-rich matrix bound by a single membrane. Their morphology, abundance and function depends on species and developmental stage [1]. Some well-known peroxisomal functions include fatty acid oxidation and hydrogen peroxide detoxification, but many more exist [2]. Their importance in human health is underlined by the severe diseases such as adrenoleukodystrophy (ALD) caused by defects in peroxisome function [3].

Peroxisome function is largely determined by peroxisomal protein content. Most peroxisomal membrane proteins (PMPs) are synthesized in the cytosol and targeted directly to peroxisomes [4] although a subset of PMPs may be delivered to peroxisomes *via* the endoplasmic reticulum [5]. PMPs regulate many aspects of peroxisome biology, including peroxisomal protein import [6], peroxisome numbers [7] and small molecule transport into peroxisomes [8]. For peroxisome function, PMP homeostasis is vital; this includes the regulation of targeting but also protein quality control processes and protein degradation. Recently, we demonstrated that the PMPs Pex3p and Pex13p in the yeast *Hansenula polymorpha* are actively down-regulated [9,10]. Pex3p degradation initiates selective autophagy of peroxisomes while Pex13p degradation is linked to peroxisomal matrix protein import. Both Pex3p and Pex13p are degraded by the Ubiquitin Proteasome System (UPS) [11]. In this system, ubiquitin (Ub) is activated by a ubiquitin-activating enzyme (E1), then transferred to the active site cysteine of an ubiquitin-conjugating enzyme (E2) and finally, Ub is attached to the substrate with the aid of an ubiquitin ligase (E3) [12–14]. Three classes of E3s exist. HECT E3 ligases accept Ub onto an active site cysteine and then transfer Ub to a substrate [15,16], whereas RING E3 ligases act as bridge between E2 and substrate, allowing Ub transfer to occur [17,18]. The third class of E3 ligase, known as RING-in-between-RING (RBR) E3s, contain a RING domain, followed by an RBR domain and finally a RING-like domain [19]. These RBR E3s, like

* Corresponding author.
E-mail address: c.p.williams@rug.nl (C. Williams).

https://doi.org/10.1016/j.bbamem.2020.183342
Received 5 February 2020; Received in revised form 2 May 2020; Accepted 4 May 2020
Available online 13 May 2020

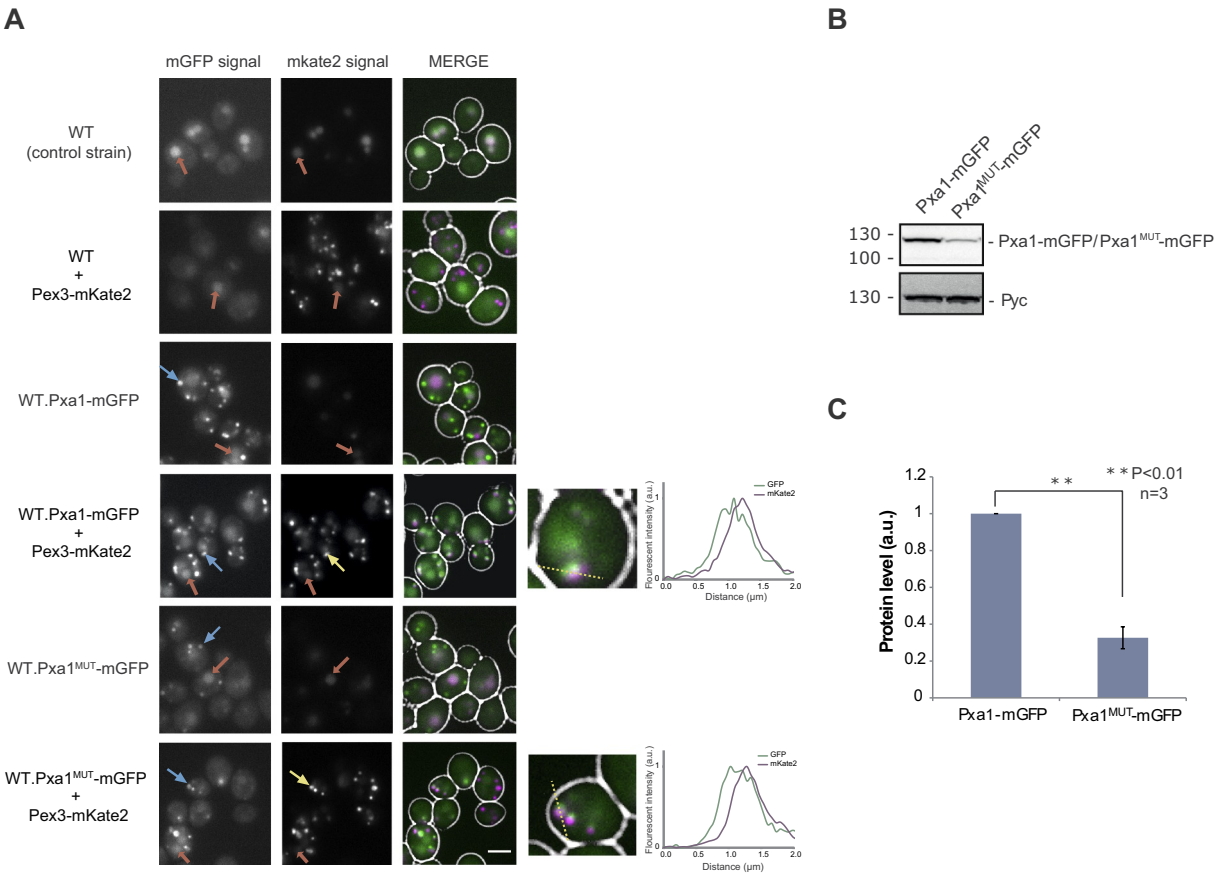

Fig. 1. Pxa1^{MUT}-mGFP targets to peroxisomes but displays reduced protein levels.
A Pxa1-mGFP and Pxa1^{MUT}-mGFP localization in cells co-expressing Pex3-mKate2 (row 4 and 6). Cells pre-cultivated on glucose were grown on oleate/glucose media to an OD_{600} of 1.5 and fluorescence images were taken. Here, a WT strain lacking fluorescent markers (row 1) together with WT strains expressing only Pex3-mKate2 (row 2), Pxa1-mGFP (row 3) or Pxa1^{MUT}-mGFP (row 5) act as controls. Blue arrows- GFP spots, yellow arrows- mKate2 spots and red arrows- background fluorescence. The line profiles (taken from the spots indicated with blue or yellow lines in images of WT.Pxa1-mGFP + Pex3-mKate2 and Pxa1^{MUT}-mGFP + Pex3-mKate2 cells) indicate normalized fluorescent intensity along a line drawn through the peroxisomes (dotted yellow line). Scale bar: 3 μm.
B Cells expressing Pxa1-mGFP or Pxa1^{MUT}-mGFP were grown on oleate/glucose media to an OD_{600} of 1.5, lysed and samples were subjected to SDS-PAGE and immunoblotting with antibodies against mGFP and Pyc.
C Bar chart displaying Pxa1-mGFP and Pxa1^{MUT}-mGFP levels, normalized to the loading control Pyc. Protein levels in Pxa1-mGFP cells were set to 1. Values represent the mean ± SD of three independent experiments. Here, asterisks represent statistically significant decrease in Pxa1^{MUT}-mGFP levels compared to Pxa1-mGFP levels. For quantification, blots in Fig. S1C were used. (For interpretation of the references to colour in this figure legend, the reader is referred to the web version of this article.)

HECT E3s, accept Ub from an E2 onto a cysteine in the RING-like domain before transferring it to the substrate [20].

The examples of Pex3p and Pex13p demonstrate that targeted down-regulation of PMPs does occur. However, because peroxisomes are involved in various oxidative metabolic reactions, they can generate large amounts of reactive oxygen species (ROS) such as hydrogen peroxide [21]. Because ROS are toxic compounds which cause damage to biomolecules [22], it is highly likely that PMPs residing in the ROS rich environment of the peroxisome undergo oxidative damage. Therefore, PMP quality control is likely to play a vital role in peroxisome biology yet to date little is known on how misfolded, non-functional or faulty PMPs are targeted for degradation *via* quality control. Here we have investigated PMP quality control in the yeast *Saccharomyces cerevisiae* using Pxa1p as substrate. Pxa1p is a half-ABC transporter, containing six transmembrane helices and a nucleotide-binding domain (NBD). The hetero-dimerization of Pxa1p with Pxa2p, another half-ABC transporter, is required for transporting acyl-CoA such as Oleoyl-CoA into peroxisomes [23,24]. Pxa1p is the homologue of human adrenoleukodystrophy protein (ALDP) [25]. Mutations in ALDP cause ALD [26] and many ALDP mutants are rapidly degraded, likely by the proteasome [27]. This has led to the suggestion that blocking ALDP degradation might constitute a feasible therapeutic approach to treat ALD [27,28]. However, to date little is known about the mechanisms underlying ALDP instability or degradation.

Using a mutant form of Pxa1p (Pxa1^{MUT}) that mimics ALD-causing ALDP mutations, fused to mGFP, we show that Pxa1^{MUT}-mGFP is rapidly degraded from peroxisomes. Furthermore, we show that Pxa1^{MUT}-mGFP degradation is dependent on the proteasome while our data also demonstrate a role for the E3 ligase Ufd4p in Pxa1^{MUT}-mGFP degradation. Finally, we show that inhibiting Pxa1^{MUT}-GFP degradation partially restores Pxa1p function *in vivo*. Taken together, our study demonstrates that faulty PMPs can undergo proteasome-mediated degradation. Furthermore, our observations on Pxa1^{MUT}-mGFP degradation may provide new insights into the role of ALDP stability in ALD.

2. Results

2.1. Pxa1^{MUT}-mGFP undergoes proteasome-mediated degradation from peroxisomes

Unlike wild-type (WT) ALDP, many mutant versions of ALDP are unstable and are rapidly degraded [29,30], suggesting that quality

control of faulty peroxisomal fatty acid transporters occurs. To investigate this in *S. cerevisiae*, we chose to study the degradation of the yeast ALDP homologue Pxa1p. For this, we selected two ALD causing mutations in ALDP, a commonly occurring glycine to serine substitution at position 512 (p.Gly512Ser) together with a lysine to arginine substitution at position 513 (p.Lys513Arg), both present in the walker A motif of the NBD (www.adrenoleukodystrophy.info). The p.Gly512Ser mutation causes reduced protein stability *in vivo* [31] although importantly, it does not abolish ATP-hydrolysis activity *in vitro* [32]. The p.Lys513Arg mutation also causes protein instability *in vivo* (www.adrenoleukodystrophy.info). The corresponding ALDP mutations (p.Gly650Ser and p.Lys651Arg) were both introduced into yeast *PXA1*. We chose to introduce two mutations to maximize the destabilizing effect to Pxa1p. The Gly650Ser/Lys651Arg mutant form of Pxa1p is referred to as Pxa1^{MUT}. We choose to fuse Pxa1^{MUT} to mGFP (Pxa1^{MUT}-mGFP), which allowed us to follow Pxa1^{MUT} using both biochemical and microscopy based techniques. Furthermore, the DNA encoding for Pxa1^{MUT}-mGFP was integrated into the genome of the *S. cerevisiae* strains used and therefore represents the only copy of *PXA1* in the cells.

Since Pxa1p functions in transporting fatty acyl-CoA, such as Oleoyl-CoA, into peroxisomes for β-oxidation [23,24], we performed all our experiments using cells grown on oleate containing media, to better understand the turnover of Pxa1^{MUT}-mGFP under conditions when the protein is required. For this purpose, *S. cerevisiae* cells were pre-cultivated on glucose medium and shifted to oleate medium, to induce the expression of the proteins required for peroxisomal β-oxidation [33–35]. However, because we performed experiments using deletion mutants that are unable to utilize oleate as carbon source (see below), we used oleate medium containing 0.1% glucose throughout the study, to allow results to be comparable. Therefore unless otherwise stated, oleate medium always contained 0.1% glucose.

First, we investigated whether Pxa1^{MUT}-mGFP is properly targeted to peroxisomes. For this, we used fluorescence microscopy to examine the localization of Pxa1^{MUT}-mGFP in cells grown on oleate. Pex3-mKate2 (Fig. 1A) or DsRed-SKL (Fig. S1A) was used as a marker for peroxisomes. As control, we used cells producing an mGFP-tagged version of WT Pxa1p (Pxa1-mGFP). We observed that mGFP spots co-localized with mKate2 spots in strains expressing Pxa1-mGFP (Fig. 1A, row 4) or Pxa1^{MUT}-mGFP (Fig. 1A, row 6) while line profile data indicate a strong correlation between the normalized fluorescent intensity of mGFP and mKate2 (Fig. 1A, row 4 and row 6, right), indicating that both Pxa1-fusions correctly target to peroxisomes. Likewise, mGFP spots co-localized with DsRed spots in cells expressing Pxa1^{MUT}-mGFP and DsRed-SKL (Fig. S1A), confirming that Pxa1^{MUT}-mGFP correctly targets to peroxisomes. We also observed larger, more diffuse spots in both mGFP and mKate2 channels (Fig. 1A, red arrows). However, these were also seen in WT cells lacking fluorescent markers (Fig. 1A, row 1) and likely represent auto-fluorescence.

The mGFP signal in cells expressing Pxa1^{MUT}-mGFP was lower and fewer GFP spots were visible compared to those expressing Pxa1-mGFP (Fig. 1A, row 6), which is consistent with the reduced protein levels of Pxa1^{MUT}-mGFP compared to those of Pxa1-mGFP (Figs. 1B, C and S1C). Lower protein levels could suggest either reduction in protein production or reduced protein stability. To examine the stability of Pxa1^{MUT}-mGFP we performed chase analysis using the protein synthesis inhibitor cycloheximide (CHX). For this purpose, cells were pre-cultivated on glucose, transferred to oleate containing media (peroxisome inducing conditions) and grown for 11 h until an OD_{600} of ~1.5. After 11 h of growth in oleate containing media, cells were treated with either CHX or DMSO (control), cells were grown further for 6 h (Pxa1-mGFP) or 2 h (Pxa1^{MUT}-mGFP) on inducing medium and samples were collected for western blotting.

We observed an increase in Pxa1-mGFP and Pxa1^{MUT}-mGFP levels in DMSO-treated cells over time (Fig. 2A, DMSO), consistent with the observation that Pxa1-mGFP levels continue to increase until ~36 h after transfer of cells to induction medium (Fig. S1D). Significantly, Pxa1^{MUT}-mGFP was rapidly degraded and displayed a significantly shorter half-life (~15 min) compared to Pxa1-mGFP (~360 min or 6 h) (Fig. 2A, CHX and S1E) in cells treated with CHX, indicating that the mutations introduced into Pxa1p result in protein instability.

Next, we sought to determine whether Pxa1^{MUT}-mGFP degradation occurs after targeting to peroxisomes. For this, we imaged CHX treated WT cells co-expressing Pex3-mKate2 and Pxa1-mGFP or Pxa1^{MUT}-mGFP. We observed that the number of mGFP positive spots reduced over time in cells expressing Pxa1^{MUT}-mGFP (Fig. 2B, right panel) while cells expressing Pxa1-mGFP displayed many more mGFP positive spots after 120 min of CHX treatment (Fig. 2B, left panel). The number of mKate2 spots remained stable after CHX treatment in both strains (Fig. 2B). These observations suggest that Pxa1^{MUT}-mGFP is degraded from peroxisomes. To validate this further, we quantified mGFP and mKate2 fluorescence intensities on peroxisomes in our fluorescent images. We observed that, as expected, the mKate2 intensity remained stable over time in the two strains (Fig. 2C). Likewise, the mGFP intensity on peroxisomes in CHX-treated Pxa1-mGFP cells remained stable (Fig. 2C, left panel) but decreased rapidly in Pxa1^{MUT}-mGFP cells treated with CHX (Fig. 2C, right panel). In addition, the mGFP/mKate2 ratio in CHX treated Pxa1^{MUT}-mGFP cells decreased rapidly over time but remained stable in Pxa1-mGFP cells after CHX addition (Fig. 2D). The rate of the decrease in mGFP intensity in Pxa1^{MUT}-mGFP cells treated with CHX appears different from that obtained using western blotting (Fig. 2A), likely due to the high background observed in the mGFP channel (Fig. 1A, row 1 and 2). Together, these data strongly suggest that Pxa1^{MUT}-mGFP is rapidly degraded from peroxisomes.

Since ALDP mutants are thought to be degraded *via* the proteasome [30], we first examined whether the proteasome has a role in Pxa1^{MUT}-mGFP degradation, through the use of a mixture of the proteasome inhibitors MG132 and Bortezomib (Figs. 3A and S1F). We assessed Pxa1^{MUT}-mGFP turnover in cells lacking Pdr5p (the major drug efflux transporter [36]), to enhance the uptake of inhibitors [37,38]. In addition, we examined Pxa1^{MUT}-mGFP degradation in cells lacking Atg12p (Figs. 3B and S1G), which is involved in autophagy [39]. From our CHX chase analysis, we observed that Pxa1^{MUT}-mGFP degradation is inhibited in *pdr5* cells after the addition of proteasome inhibitors (Fig. 3A, CHX+ MG132 + Bortezomib) compared to non-treated cells (Fig. 3A, CHX). These data, together with the observation that the deletion of *ATG12* had no effect on Pxa1^{MUT}-mGFP turnover (Figs. 3B and S1G) demonstrates that the proteasome is involved in Pxa1^{MUT}-mGFP degradation. Next, we checked whether ubiquitination has a role in Pxa1^{MUT}-mGFP degradation by expressing a mutant form of ubiquitin (Ub^{K48R}) in Pxa1^{MUT}-mGFP cells, to inhibit poly-ubiquitin chain formation on the substrate and subsequent degradation by the proteasome [40]. We observed that Pxa1^{MUT}-mGFP turnover is reduced in cells expressing Ub^{K48R}, compared to Ub expressing cells (Figs. 3C and S1G). However, we were unable to detect ubiquitinated Pxa1^{MUT}-mGFP (Fig. 3D). Possibly ubiquitinated Pxa1^{MUT}-mGFP is below the level of detection because of the high speed by which Pxa1^{MUT}-mGFP is degraded. In summary, these data demonstrate that Pxa1^{MUT}-mGFP undergoes rapid, proteasome-mediated degradation from peroxisomes.

2.2. Identifying components required for Pxa1-tFT degradation

To gain the first insights into mechanisms of Pxa1^{MUT}-mGFP quality control, we set out to identify components required for Pxa1^{MUT}-mGFP degradation using a tandem fluorescent protein timer (tFT). A tFT is a fusion of two fluorescent proteins; the slow maturing mCherry and the rapid maturing sfGFP (Fig. 4A). When tagged to a protein of interest, the mCherry/sfGFP ratio provides information on protein stability. tFT fusions undergoing fast turnover are degraded prior to mCherry maturation, resulting in a low mCherry/sfGFP ratio, whereas the mCherry/sfGFP ratio increases for proteins with slower turnover [41]. Similar to Pxa1^{MUT}-mGFP, Pxa1-tFT levels in cells were much lower compared to Pxa1-mGFP levels (Fig. 4B) while Pxa1-tFT was rapidly degraded in

cells treated with CHX (Figs. 4C and S1H). The turnover of tFT-tagged Pex11p, a stable PMP [9], was slower in comparison (Figs. 4C and S1H). Furthermore, the GFP immunoreactive band at around 33 kDa observed with samples containing Pxa1-tFT (Figs. 4B and S1H, marked **) is derived from incomplete tFT processing by the proteasome [42], suggesting a role for the proteasome in Pxa1-tFT turnover. From these data, we conclude that, similar to Pxa1^{MUT}-mGFP, Pxa1-tFT undergoes proteasome-mediated degradation and for this reason, we did not create a Pxa1-tFT fusion containing the Gly650Ser/Lys651Arg mutations.

Next, we investigated the stability of Pxa1-tFT in a library of 132 strains that lack a protein involved in protein degradation or which contained a mutant version of a protein involved in protein degradation (in case the deletion was lethal) using a synthetic genetic array [43,44]. This library represents a large fraction of the factors known to have a role in the degradation of proteins in yeast (see Table S2 for details on which strains were included in the library). The effect of the mutations on the stability of Pxa1-tFT was examined using mCherry/sfGFP intensity ratios obtained from whole colonies after one, two and three

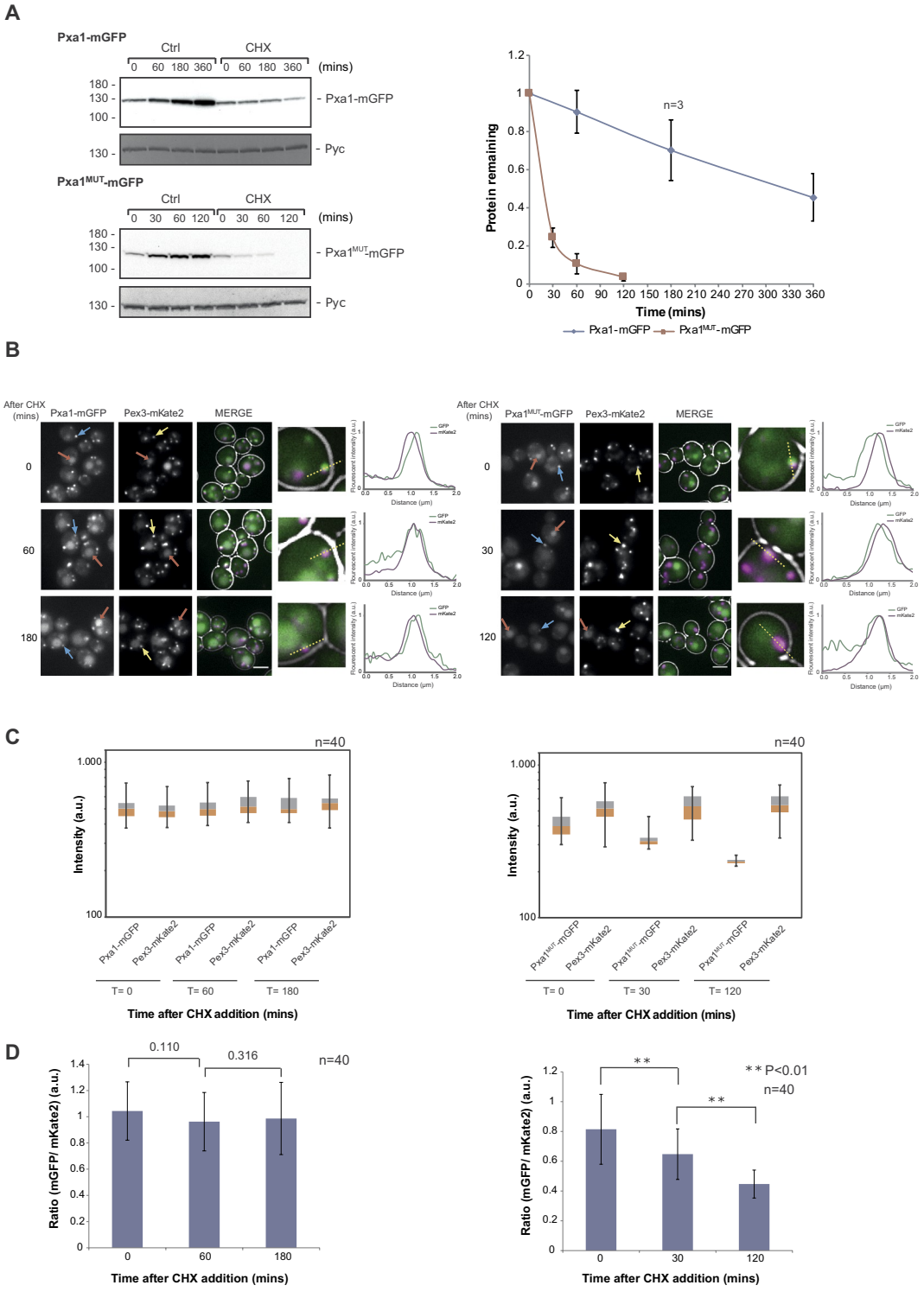

(caption on next page)

Fig. 2. Pxa1^{MUT}-mGFP is rapidly degraded from peroxisomes.
A Cycloheximide (CHX) chase analysis on cells expressing Pxa1-mGFP and Pxa1^{MUT}-mGFP. (Left) Cells pre-cultivated on glucose media were grown on oleate/glucose media (inducing condition) to an OD_{600} of 1.5. After treatment with DMSO (Ctrl) or CHX, cells were grown further on inducing medium and samples were collected at the indicated time points for immunoblotting with antibodies against mGFP and Pyc. (Right) Quantification of Pxa1-mGFP and Pxa1^{MUT}-mGFP levels after CHX addition. Protein levels were normalized to Pyc at the corresponding time point and to the protein levels at time point 0 (set to 1). Values represent the mean ± SD of three independent experiments. For quantification, blots in Fig. S1E were used.
B Co-localization analysis of Pxa1-mGFP (Left) and Pxa1^{MUT}-mGFP (Right) with the peroxisomal marker Pex3-mKate2 after CHX treatment. Cells expressing Pxa1-mGFP or Pxa1^{MUT}-mGFP together with Pex3-mKate2 were grown on oleate/glucose media to an OD_{600} of 1.5 and treated with CHX. Fluorescence images were taken from cells grown on oleate/glucose media at the indicated time points (min) after CHX addition. Blue arrows- GFP spots, yellow arrows- mKate2 spots and red arrows- background fluorescence. Scale bar: 3 μm. Line profiles were generated as described in Fig. 1.
C Box plot quantification of mGFP and mKate2 fluorescence intensity at the peroxisomal membrane in WT cells producing Pex3-mKate2 and Pxa1-mGFP (Left) or Pxa1^{MUT}-mGFP (Right) after CHX treatment. Fluorescence intensities were measured in cells ($n = 40$) using ImageJ as described in the materials and methods section. The box represents intensity values from the 25th percentile to the 75th percentile. The orange area represents intensity values from the 25th -50th percentile and the grey area represents intensity values from the 50th -75th percentile. Whiskers indicate maximum and minimum values.
D Average ratio ± SD per cell (n = 40) of mGFP to mKate intensities in WT cells producing Pex3-mKate2 and Pxa1-mGFP (Left) or Pxa1^{MUT}-mGFP (Right). Numbers above the columns (Left) depict the *p*-value. Asterisks (Right) denote significance between ratios at different time points, ** $P < 0.01$- statistically significant (Right) and $P > 0.05$- not significant (Left). (For interpretation of the references to colour in this figure legend, the reader is referred to the web version of this article.)

days of growth on oleate/glucose plates. These mCherry/sfGFP ratios were used to calculate a heat map of *Z*-scores (Fig. 4D), which depicts the stability of Pxa1-tFT in each strain. A strain displaying similar Pxa1-tFT stability as in WT cells would have a Z-score of 0 while strains with enhanced stability would exhibit a Z-score > 0 (see Materials and methods). Mutant strains that displayed an increase in Z-score > 1.0 on two of the three days tested were considered as potential candidates that increased Pxa1-tFT stability. Pxa1-tFT stability was increased in cells lacking functional proteasomes (*pre2*, *pre6*, *rpn10*, *rpt6-25* and *ubp6* cells) but not in cells lacking Atg12p (Fig. 4D), confirming a role for the proteasome in Pxa1-tFT stability. These results demonstrate that our tFT analysis is a valid way to identify factors potentially involved in Pxa1^{MUT}-mGFP degradation.

Pxa1-tFT stability was increased in strains deleted for genes coding for the peroxisomal E2 Pex4p or one of the three peroxisomal E3 ligases Pex2p, Pex10p and Pex12p [45] (Fig. 4D). Consistent with this, Pxa1-tFT protein levels were enhanced in *pex2* and *pex4* cells (Fig. 4E), thereby confirming our tFT data. Roles for these proteins in PMP ubiquitination/degradation have already been reported [9,10,46], suggesting that common mechanisms may govern PMP ubiquitination and degradation. However, Pxa1-tFT stability was also enhanced in cells lacking a number of de-ubiquitinating enzymes (DUBs), which could suggest a role for these DUBs in the deubiquitination of Pxa1^{MUT}-mGFP prior to proteasomal degradation. In addition, cells lacking the E3s Nam7p, Dma2p, Tul1p and Ufd4p, the E3 co-factor proteins Ela1p and Skp2p and the ubiquitin-binding protein Dsk2p (Supplementary Table S2), factors not previously associated with peroxisomes, also displayed enhanced Pxa1-tFT stability. Overall, our tFT analysis identified factors potentially involved in the degradation of faulty Pxa1p.

2.3. Components involved in Pxa1-tFT stability play a role in Pxa1^{MUT}-mGFP degradation

Previously we demonstrated that the peroxisomal ubiquitination machinery is required for the degradation of the PMPs Pex3p and Pex13p [9,10]. Because deletion of *PEX4*, *PEX2*, *PEX10* or *PEX12* results in Pxa1-tFT stabilization (Fig. 4D and E), we were interested to investigate whether they also had a role in Pxa1^{MUT}-mGFP degradation. Indeed, Pxa1^{MUT}-mGFP levels were enhanced in cells deleted for *PEX2* or *PEX4* (Figs. 5A and S2A) while Pxa1^{MUT}-mGFP turnover was also inhibited in these cells (Figs. 5B and S2B), validating our tFT data as well as indicating a role for these peroxisomal proteins in Pxa1^{MUT}-mGFP degradation. Furthermore, Pxa1^{MUT}-mGFP localized to peroxisomes in these strains (Fig. 5C), indicating that stabilization did not arise from mistargeting to other cell compartments. However, because cells deleted for *PEX2* or *PEX4* also lack functional peroxisomes [47], we investigated the impact of peroxisome function alone on Pxa1^{MUT}-mGFP turnover by assessing the stability and turnover of Pxa1^{MUT}-mGFP in *pex5* cells, which also lack functional peroxisomes [48]. Our data demonstrate that Pxa1^{MUT}-mGFP degradation was inhibited in *pex5* cells (Figs. 5A, B and S2B), suggesting that Pxa1^{MUT}-mGFP degradation may be linked to peroxisome function. Again, Pxa1^{MUT}-mGFP targeting was not impaired in *pex5* cells (Fig. 5C). We observed that Pex3-mKate2 levels are comparable in WT, *pex2*, *pex4* and *pex5* cells (Fig. S2C), suggesting that the effect of these deletion strains is not general for all PMPs. Nevertheless, these data indicate that studying Pxa1^{MUT}-mGFP turnover in strains deficient in peroxisome function could be challenging because any effects may potentially be indirect.

Therefore, we turned to investigate the role of candidates identified in our tFT analysis not previously associated with peroxisome function, including Ufd4p, Nam7p, Ela1p, Dsk2p, Skp2p, Tul1p and Dma2p. Interestingly, we observed that Pxa1^{MUT}-mGFP levels were significantly higher in cells lacking Ufd4p (Figs. 6A and S2A). Deletion of *ELA1*, *DSK2*, *SKP2*, *TUL1* or *DMA2* did not impact significantly on Pxa1^{MUT}-mGFP levels (Figs. 6A and S2A) and were not investigated further. Furthermore, Pxa1^{MUT}-mGFP levels were significantly lower in the *NAM7* deletion strain compared to the WT (Figs. 6A and S2A). However, because we were specifically interested in UPS mutants that increased the stability of Pxa1^{MUT}-mGFP, the role of *NAM7* in Pxa1^{MUT}-mGFP stability was not investigated further.

Significantly, we observed that *ufd4* cells retain the ability to grow on media containing oleate as sole carbon source (Fig. 6B), indicating that they contain functional peroxisomes and hence that Pxa1^{MUT}-mGFP stabilization in this strain does not stem from a deficiency in peroxisome function. Since Ufd4p is a cytosolic E3 ligase that regulates the degradation of faulty proteins [49], but it has not been linked to peroxisome function, we chose to investigate the role of Ufd4p in Pxa1^{MUT}-mGFP degradation further. We performed CHX chase analysis and observed that Pxa1^{MUT}-mGFP degradation is inhibited in *ufd4* cells compared to WT cells (Figs. 6C and S2B). Furthermore, using fluorescence microscopy in combination with CHX chase assays, we investigated the localization and turnover of Pxa1^{MUT}-mGFP in *ufd4* cells. As can be seen in Fig. 6D ($t = 0$, left panel), mGFP spots co-localize with mKate2 spots in *ufd4* cells. In addition, line profile data indicate strong correlation between the normalized fluorescent intensity of mGFP and mKate2, demonstrating that Pxa1^{MUT}-mGFP is indeed localized to peroxisomes in *ufd4* cells (Fig. 6D). The peroxisomal localisation of Pxa1^{MUT}-mGFP in *ufd4* cells was confirmed using DsRed-SKL as a peroxisomal marker (Fig. S1A). Significantly, cells deleted for *UFD4* display increased numbers of mGFP spots after 120 min of CHX treatment, compared to the WT strain (Fig. 6D, right panel; $t = 120$ min). Furthermore, mGFP spots in *ufd4* cells co-localize with mKate2 spots after 120 min of CHX treatment (Fig. 6D, left panel), demonstrating that Pxa1^{MUT}-mGFP accumulates on peroxisomes in these cells. Together, these data establish that the E3 ligase Ufd4p is involved in the proteasome-dependent degradation of Pxa1^{MUT}-mGFP.

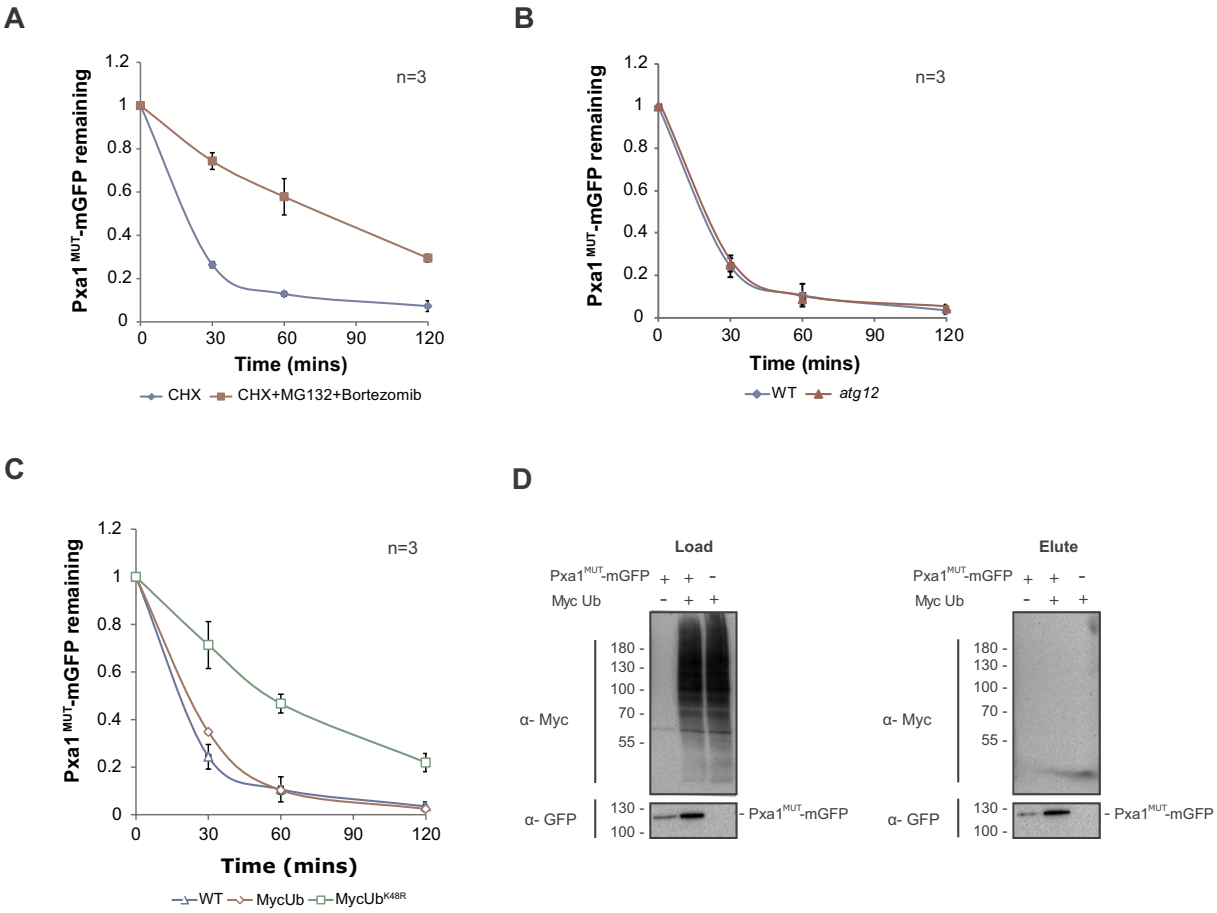

Fig. 3. Inhibiting the proteasome but not autophagy disturbs Pxa1^{MUT}-mGFP degradation

A Graph representing Pxa1^{MUT}-mGFP levels in *pdr5* cells under proteasome inhibitor (PI) conditions. *pdr5* cells expressing Pxa1^{MUT}-mGFP pre-cultivated on glucose were grown on oleate/glucose media for 10 h. After incubation with DMSO or proteasome inhibitors (MG132 and Bortezomib) for 90 min, CHX was added to DMSO (represented as CHX) and PI treated cells (denoted as CHX + MG132 + Bortezomib). TCA samples for western blotting were collected from cells grown on oleate/glucose media at the indicated time points after treatment with inhibitors. Protein levels were normalized to Pyc at the corresponding time point and to the protein levels at time point 0 (set to 1). Values represent the mean ± SD of three independent experiments. For quantification, blots in Fig. S1F were used.

B Pxa1^{MUT}-mGFP levels in WT and *atg12* cells after CHX treatment. Cells pre-cultivated on glucose were grown on oleate/glucose media to an OD_{600} of 1.5 and treated with CHX. TCA samples were collected from cells grown on oleate/glucose at the indicated time points after CHX treatment and probed with western blotting. Protein levels were normalized to Pyc at the corresponding time point and to the protein levels at time point 0 (set to 1). For quantification, blots in Fig. S1G were used.

C Quantification of Pxa1^{MUT}-mGFP levels in WT cells and cells expressing Myc-tagged ubiquitin (Ub) or ubiquitin mutant (Ub^{K48R}) after treatment with CHX. The experiment and quantification of levels were performed as mentioned in Fig. 3B. Values represent the mean ± SD of three independent experiments. For quantification, blots in Fig. S1G were used.

D Immunoprecipitation performed using anti-GFP antibodies on lysates from *pdr5* cells, *pdr5*.Pxa1^{MUT}-mGFP cells, *pdr5*.Pxa1^{MUT}-mGFP/MycUb cells and *pdr5*.MycUb cells. Cells were pre-cultivated on glucose, transferred to oleate/glucose media for 10 h and incubated with proteasome inhibitors (MG132 and Bortezomib) for 90 min. Pxa1^{MUT}-mGFP was immunoprecipitated under native conditions using GFP-trap magnetic beads. Load and elute fractions were subjected to immunoblotting with antibodies against the Myc-tag (to detect Myc-ubiquitin) or the GFP-tag (to detect Pxa1^{MUT}-mGFP).

2.4. Inhibiting Pxa1^{MUT}-mGFP degradation enhances peroxisomal β-oxidation

Around 70% of the mutant forms of ALDP are unstable and are degraded [30,50]. However, many of these mutants retain a certain level of functionality [32]. This has led to the hypothesis that blocking ALDP degradation could enhance ALDP activity in cells and be beneficial for ALD patients [27–29]. Our data clearly indicate that Pxa1^{MUT}-mGFP builds up at peroxisomes when its degradation is inhibited in *ufd4* cells. Hence, we reasoned that we could use our experimental setup as proof of principle and measured the capacity of WT and *ufd4* cells expressing Pxa1-mGFP or Pxa1^{MUT}-mGFP to perform β-oxidation (Fig. 7A). Pxa1^{MUT}-mGFP in WT cells displayed reduced activity in comparison to Pxa1-mGFP (Fig. 7A) although higher than *pxa1* cells, indicating that importantly, Pxa1^{MUT}-mGFP retains a degree of functionality. Significantly, *ufd4* cells expressing Pxa1^{MUT}-mGFP exhibited an increase in β-oxidation activity of around 15% compared to the activity of WT.Pxa1^{MUT}-mGFP cells (Fig. 7A). We also observed that β-oxidation appeared enhanced in *ufd4* cells expressing Pxa1-mGFP compared to WT cells, although statistical analysis suggested that this increase was not significant (Fig. 7A). To investigate further, we determined the levels of Pxa1-mGFP in WT and *ufd4* cells expressing Pxa1-mGFP (Fig. 7B), observing that these levels were indeed increased in *ufd4* cells. Significantly, Pex14p levels were not affected by *ufd4* deletion (Fig. 7B), indicating that the effect is likely to be specific for Pxa1-mGFP.

Overall, our results provide proof of principle that blocking Pxa1^{MUT}-mGFP degradation can partially restore Pxa1^{MUT}-mGFP function in cells, supporting the view that inhibiting ALDP degradation may be a promising therapeutic avenue to explore to target ALD.

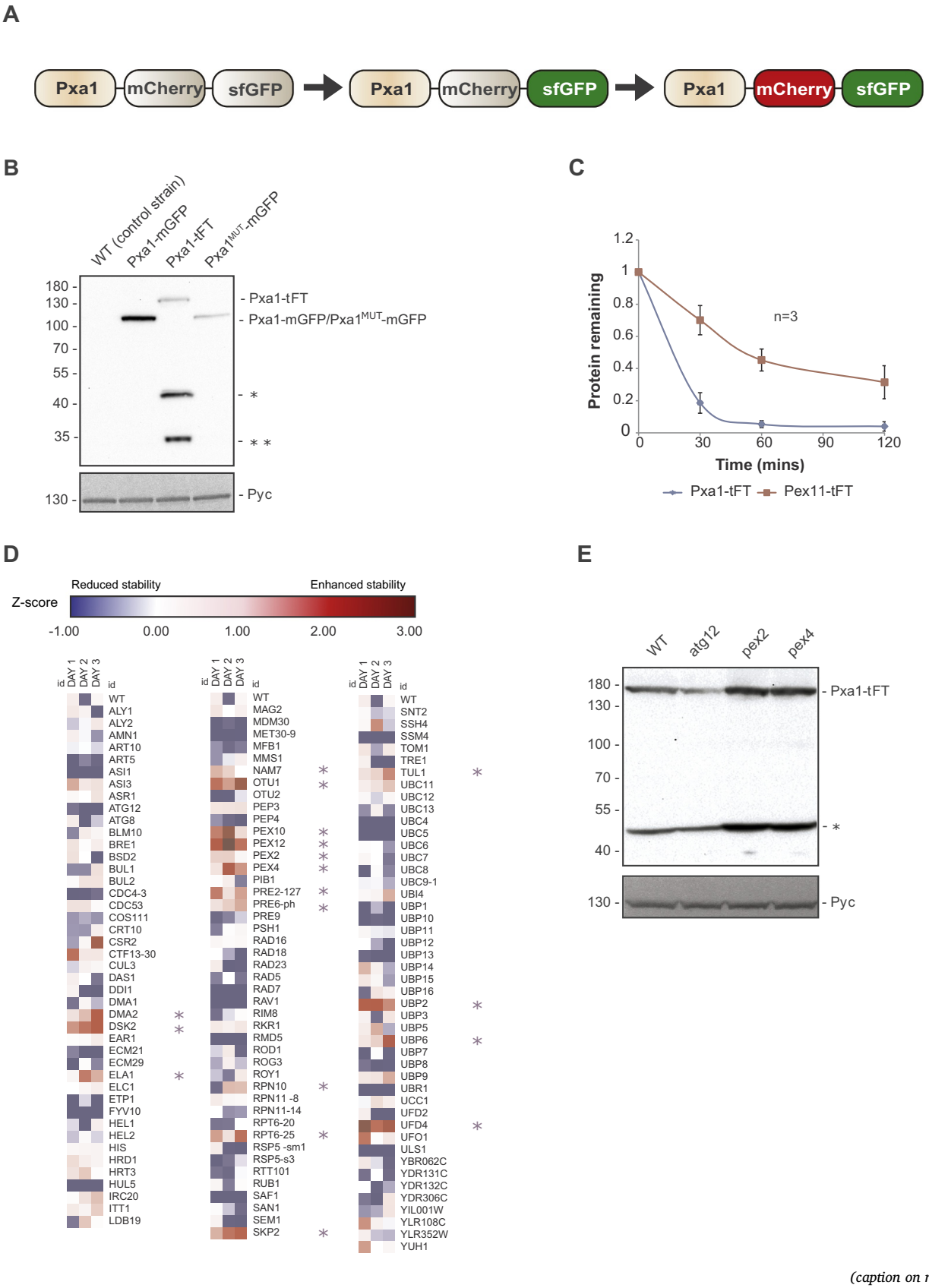

(caption on next page)

Fig. 4. Identifying factors involved in Pxa1^{MUT}-tFT degradation by tandem fluorescent timer.
A Schematic representation of the Pxa1-tandem fluorescent timer (tFT) fusion. Pxa1p is fused to two fluorescent proteins with different maturation kinetics: rapidly maturing sfGFP and slow maturing mCherry. The fluorescent intensity ratio of mCherry to sfGFP provides information of Pxa1p stability.
B WT cells together with cells expressing Pxa1-mGFP, Pxa1-tFT or Pxa1^{MUT}-mGFP were initially grown on glucose, shifted to oleate/glucose media and grown until an OD_{600} of 1.5. After lysis, samples were probed by immunoblotting with antibodies against mGFP and Pyc. *denotes a shorter, mCherry-sfGFP product resulting from mCherry hydrolysis during TCA treatment [42,81] and ** denotes a tFT fragment produced by incomplete proteasomal processing [42].
C The stability of tFT tagged Pxa1p and Pex11p was assayed using CHX chase analysis. Cells pre-cultivated on glucose were grown on oleate/glucose media an OD_{600-} 1.5. After treatment with CHX, cells were further grown on oleate/glucose media and samples collected at the indicated points were subjected for western blotting. Protein levels obtained at each time point were normalized to Pyc at the corresponding time point and to the protein levels at time point 0 (set to 1). Values represent the mean ± SD of three independent experiments. For quantification, blots in Fig. S1H were used.
D Screen for components involved in Pxa1-tFT stability. WT and mutant cells expressing Pxa1-tFT were grown on oleate/glucose plates and fluorescent intensities were measured. The resulting mCherry/sfGFP ratio on the indicated days (1–3) were used to calculate the *Z*-score (see materials and methods). Z-score colour coded from blue (decrease) to red (increase), represents changes in Pxa1-tFT stability. Mutant strains with Z-score > 1.0 (indicated by *) on two of the three days tested were defined as potentially interesting.
E Western blot analysis of Pxa1-tFT levels in WT, *atg12*, *pex2* and *pex4* cells grown on oleate/glucose media to an OD_{600} of 1.5. After lysis, samples were probed by immunoblotting with antibodies against mGFP and Pyc. *denotes a shorter, mCherry-sfGFP product resulting from mCherry hydrolysis during TCA lysate preparation [42]. The apparent discrepancy between the molecular weight of Pxa1-tFT in this panel and in Fig. 4B is because samples here were run onto a 7.5% acrylamide SDS-PAGE gel while samples in 4B were loaded onto a 10% acrylamide SDS-PAGE gel, resulting in a different run profile. (For interpretation of the references to colour in this figure legend, the reader is referred to the web version of this article.)

3. Discussion

Here we have demonstrated that a faulty version of the peroxisomal fatty acid transporter Pxa1p is targeted for proteasome-dependent degradation. Pxa1^{MUT}-mGFP, our chosen substrate, is rapidly degraded from peroxisomes. An important question remains how Pxa1^{MUT}-mGFP is recognized for degradation? The mutations introduced into Pxa1p (Gly650Ser/Lys651Arg) are present in the conserved walker A motif of the NBD [51]. Mutation of either these conserved lysine or glycine residues compromises both the ATP hydrolysis and substrate translocation activity of ABC transporters [52–54], including ALDP [32]. Hence, the substitutions we introduced into Pxa1^{MUT}-mGFP likely reduce ATP hydrolysis and hence transport activity, which in turn could allow Pxa1^{MUT}-mGFP to be recognized for degradation. However, Pxa1p forms a heterodimer with Pxa2p and deletion of *PXA2* decreases the stability of Pxa1p [55], indicating that Pxa2p binding is required for Pxa1p stability. Therefore, it is equally possible that the substitutions in Pxa1^{MUT}-mGFP inhibit binding to Pxa2p, which in turn allows Pxa1^{MUT}-mGFP to be recognized for degradation. Interestingly, Byeon et al. reported that mutating the walker A lysine in muscle adenylate kinase results in a conformational change in the NBD [52] while recent work on the bacterial transporter MJ0796 demonstrated that walker A lysine mutations impact on both ATP hydrolysis and homo-dimerization [54]. Hence, we speculate that the introduced mutations in Pxa1^{MUT}-mGFP result in a conformational change in Pxa1p, which could allow the protein to be recognized for degradation. Identifying which factors are involved in the recognition of faulty peroxisomal fatty acid transporters will provide valuable insights into the mechanisms underlying their degradation.

Our data show that the addition of proteasome inhibitors significantly reduce Pxa1^{MUT}-mGFP turnover, demonstrating a role for the proteasome in Pxa1^{MUT}-mGFP degradation (Fig. 3A). While the data on the ubiquitin mutant (Ub^{K48}) suggests that ubiquitination is involved in Pxa1^{MUT}-mGFP degradation (Fig. 3C), our attempts to detect ubiquitinated forms of Pxa1^{MUT}-mGFP proved unsuccessful (Fig. 3D). Notably, ubiquitinated forms of ALDP carrying the R617H or H667D mutations could also not be detected [30], even though these mutants were likely degraded by the proteasome. There could be two possible explanations for his: Pxa1^{MUT}-mGFP is ubiquitinated but that the ubiquitinated form of Pxa1^{MUT}-mGFP is below the limit of detection, or that the ubiquitination of another protein could facilitate the degradation of Pxa1^{MUT}-mGFP. The latter mode of degradation has been proposed for several substrates of the proteasome. Dang et al., reported that instead of A3G, its binding partner viral infectivity factor (Vif) undergoes poly-ubiquitination and this could be critical for A3G proteasomal degradation [56], proposing that poly-ubiquitinated Vif might act as an adaptor protein to bring A3G to the proteasome for degradation [57]. Another protein that may be degraded *via* a similar mechanism is the retinoblastoma tumour suppressor protein (Rb) [58]. Rb is thought to be targeted for proteasomal degradation by the ubiquitination of its binding partner, human papillomavirus protein E7 [58,59]. Pxa2p forms a heterodimer with Pxa1p [23,24], but we do not suspect that Pxa2p ubiquitination is required for Pxa1^{MUT}-mGFP degradation because loss of Pxa2p does not inhibit Pxa1p degradation but instead decreases the stability of Pxa1p [55]. Clearly further work is required to investigate how ubiquitin contributes to the proteasome-mediated degradation of Pxa1^{MUT}-mGFP.

Based on the results of our tFT screening, several proteins not previously associated with peroxisomal function were identified that could play a role in Pxa1-tFT stability (Fig. 4C). Of these, only loss of Ufd4p, a cytosolic E3 ligase involved in the degradation of faulty proteins [49], significantly increased the stability of Pxa1^{MUT}-mGFP (Fig. 6A), indicating that Ufd4p is involved in Pxa1^{MUT}-mGFP degradation. Although future work needs to investigate the mechanisms by which Ufd4p controls Pxa1^{MUT}-mGFP degradation, we consider it significant that a cytosolic E3 ligase could regulate the turnover of a faulty PMP because this indicates that general cellular quality control pathways can facilitate the degradation of faulty PMPs. While the data we present here concern the degradation of a mutant form of Pxa1p, we consider it unlikely that the sole purpose of PMP quality control is the degradation of mutant PMPs; we consider it more likely that damaged PMPs undergo quality control. As previously mentioned, the ROS rich environment of the peroxisome could result in the oxidative damage of proteins, which could suggest that damaged Pxa1p undergoes PMP quality control. In line with this, although Pxa1-mGFP is much more stable than Pxa1^{MUT}-mGFP in our CHX experiments, degradation of Pxa1-mGFP does occur (Fig. 2A) while Pxa1-mGFP levels are higher in *ufd4* cells compared to WT cells (Fig. 7B). Therefore, it is plausible that Pxa1^{MUT}-mGFP is targeted for degradation *via* quality control mechanisms that usually acts upon damaged Pxa1p because Pxa1^{MUT}-mGFP is impaired in function.

Deletion of *UFD4* does not fully inhibit the degradation of Pxa1^{MUT}-mGFP. Similarly, Pxa1^{MUT}-mGFP degradation appears only partly reduced in cells lacking the peroxisomal E3 ligase Pex2p. This could suggest that two pathways target Pxa1^{MUT}-mGFP for degradation, one requiring Ufd4p and the other involving Pex2p or perhaps that Pex2p and Ufd4p collaborate to facilitate Pxa1^{MUT}-mGFP degradation. Ufd4p can team up with Ubr1p, a RING E3, to facilitate the degradation of Mgt1p, a DNA repair demethylase [60]. However, the impact of peroxisome function on Pxa1^{MUT}-mGFP degradation remains to be determined, meaning that further data on the role of Pex2p (and other members of the peroxisomal ubiquitination machinery) are required to

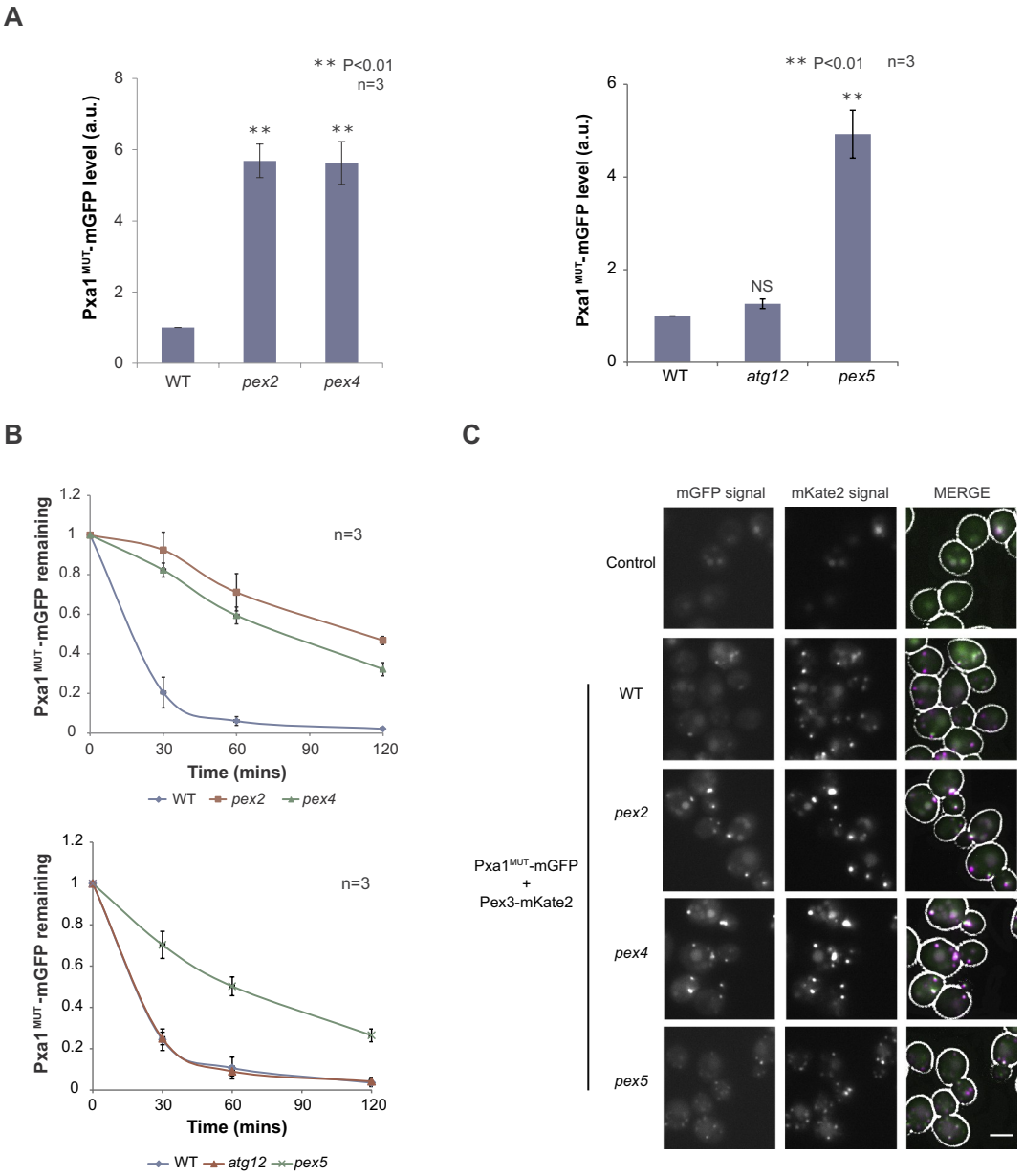

Fig. 5. Pxa1^{MUT}-mGFP degradation is inhibited in peroxisome deficient strains.

A Bar chart displaying Pxa1^{MUT}-mGFP levels in WT, *pex2* and *pex4* strains (Left) and WT, *atg12* and *pex5* strains (Right). Cells pre-cultivated on glucose were grown on oleate/glucose to an OD_{600} of ~1.5 and TCA samples were collected for western blotting. For quantification of Pxa1^{MUT}-mGFP levels, blots in Fig. S2A were used. Pxa1^{MUT}-mGFP levels in WT were set to 1, values represent the mean ± SD of three independent experiments. Asterisks represent statistically significant increase of Pxa1^{MUT}-mGFP levels in mutant strains compared to in WT cells. ** P < 0.01- statistically significant and P > 0.05- not significant (NS).

B CHX chase of Pxa1^{MUT}-mGFP in WT, *pex2* and *pex4* strains (Top) and WT, *atg12* and *pex5* strains (Bottom). Cells were grown on oleate/glucose media to an OD_{600} of 1.5, treated with CHX and samples were collected from oleate/glucose grown cells at the indicated time points after CHX treatment. Protein levels were normalized to Pyc at the corresponding time point and to the protein levels at time point 0 (set to 1). Values represent the mean ± SD of three independent experiments. For quantification, blots in Fig. S2B were used.

C Co-localization analysis of Pxa1^{MUT}-mGFP with the peroxisomal marker Pex3-mKate2 in WT, *pex2*, *pex4 and pex5* cells. The WT strain lacking fluorescent markers was used as control. Fluorescence images were taken from cells grown on oleate/glucose media to an OD_{600} of 1.5. Blue arrows- GFP spots, yellow arrows- mKate2 spots and red arrows- background fluorescence. Scale bar: 3 μm. (For interpretation of the references to colour in this figure legend, the reader is referred to the web version of this article.)

validate this hypothesis. Nevertheless, a model that depicts Pex2p and Ufd4p teaming up to degrade faulty PMPs remains an attractive one.

Mutations in gene sequences can result in formation of faulty proteins, which could pose serious threats to the cell, for two reasons. One reason is the loss of protein activity. However, there is also gain-of-toxic function that is unrelated to the protein's function and which has become increasingly relevant to human disease [61]. Faulty proteins often expose hydrophobic regions normally buried within the core [62] that may take part in unwanted protein-protein interactions, resulting in protein aggregation [63]. To minimize such harmful effects, cell employs protein quality control systems to remove faulty proteins [64]. For instance, mutations at position F508 in Cystic fibrosis transmembrane conductance regulator (CFTR), which increase the tendency of CFTR to aggregate but do not inhibit activity completely [65,66], result in rapid protein degraded [67]. However, the rapid degradation of mutant CFTR leaves cells devoid of CFTR molecules, eventually

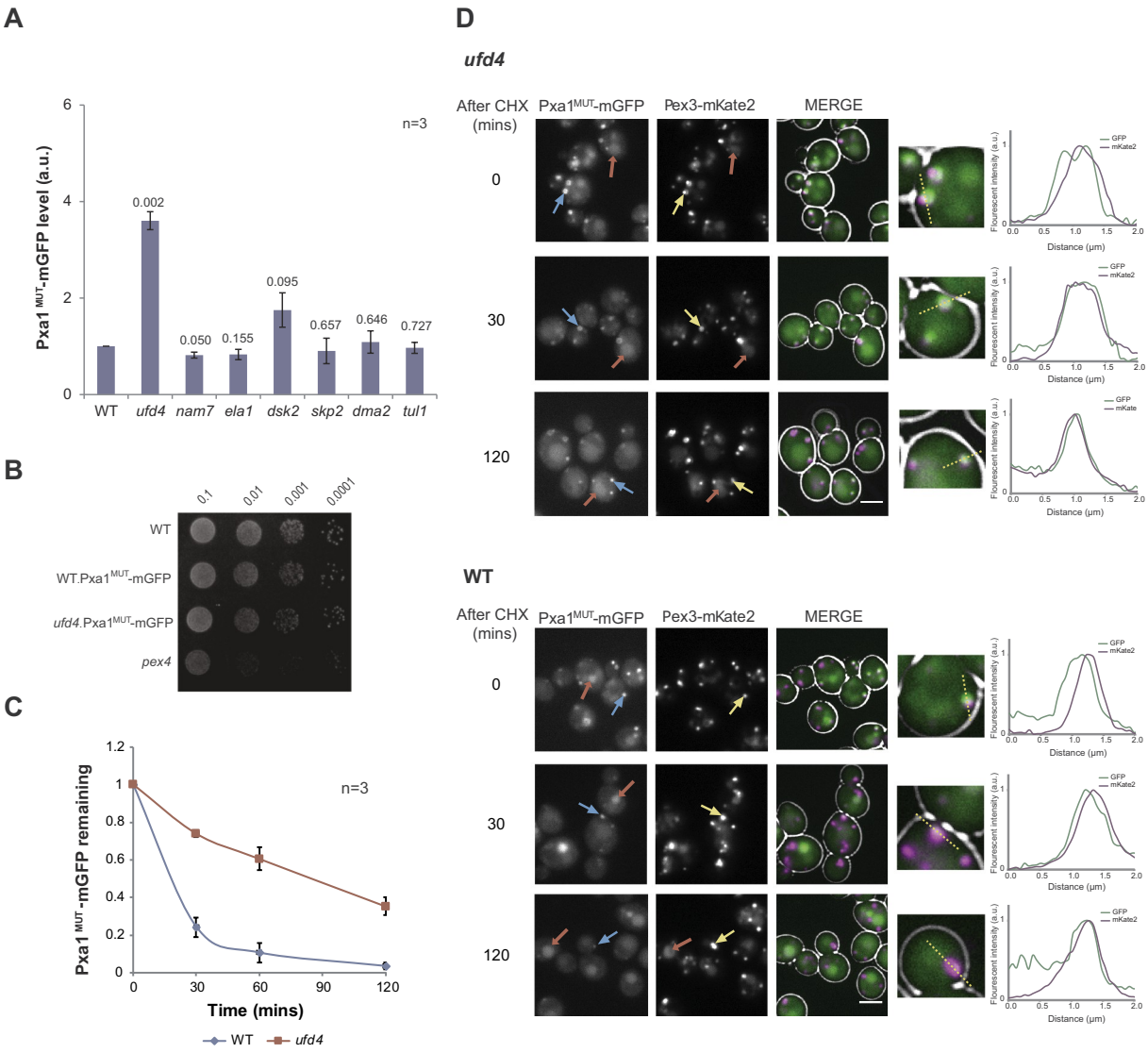

Fig. 6. Ufd4, a cytosolic E3 ligase is involved in Pxa1^{MUT}-mGFP degradation.

A Pxa1^{MUT}-mGFP levels in WT, *ufd4*, *nam7*, *ela1*, *dsk2*, *skp1*, *tul1* or *dma2* cells. TCA samples for western blotting were collected from cells pre-cultivated on glucose and grown on oleate/glucose to an OD_{600} of ~1.5. For quantification of Pxa1^{MUT}-mGFP levels, blots in Fig. S2A were used. Pxa1^{MUT}-mGFP levels in WT were set to 1, values represent the mean ± SD of three independent experiments. Numbers above the columns depict the *p*-value.

B Ten-fold serial dilutions of WT and *pex4* cells together with WT and *ufd4* cells producing Pxa1^{MUT}- mGFP were spotted on oleate plates and grown at 30 °C for 7 days.

C CHX chase of Pxa1^{MUT}-mGFP in WT and *ufd4* strains. Cells were pre-cultivated on glucose, grown on oleate/glucose to an OD_{600} 1.5, treated with CHX and samples were collected from oleate/glucose grown cells at the indicated time points after CHX addition. Protein levels were normalized to Pyc at the corresponding time point and to the protein levels at time point 0 (set to 1). Values represent the mean ± SD of three independent experiments. For quantification, blots in Fig. S2B were used.

D Co-localization analysis of Pxa1^{MUT}-mGFP with the peroxisomal marker Pex3-mKate2 in *ufd4* (Top panel) or WT (Bottom panel, taken from Fig. 2A, for comparison) cells, after CHX treatment. Cells were grown as indicated in Fig. 6C and images were taken from cells grown on oleate/glucose media at the indicated time points (min) after CHX treatment. Blue arrows- GFP spots, yellow arrows- mKate2 spots and red arrows- background fluorescence, Scale bar: 3 µm. Line profiles were generated as described in Fig. 1. The circular structures visible in GFP images of *ufd4*.Pxa1^{MUT}-mGFP cells (top panel) expressing Pxa1^{MUT}-mGFP can also be seen in images of WT.Pxa1^{MUT}-mGFP cells (Fig. S1B, top lane) and likely represent large peroxisomes. (For interpretation of the references to colour in this figure legend, the reader is referred to the web version of this article.)

resulting in the severe condition cystic fibrosis [68] and several lines of research have focused on blocking CFTR degradation as potential treatment for cystic fibrosis [69]. Similarly, many ALDP mutant proteins that cause ALD are unstable, leading to the suggestion that blocking ALDP degradation could represent a novel treatment for ALD [27]. Indeed, a subset of ALDP mutant proteins in patient cells become stable under low-temperature culture conditions and exhibit proper peroxisomal localization [27] while they also display increased residual β-oxidation activity [28]. Though unstable, a significant proportion of ALDP mutants retain a certain degree of function [27,32]. In line with this, our data demonstrate that Pxa1^{MUT}-mGFP cells display increased β-oxidation compared to *pxa1* cells (Fig. 7A), indicating that Pxa1^{MUT}-mGFP is partly functional. Furthermore, stabilizing Pxa1^{MUT}-mGFP, through the deletion of *UFD4*, enhances peroxisomal β-oxidation in cells, which would indeed support the notion that blocking ALDP mutant degradation might constitute a feasible therapeutic approach to treat ALD. However, Yamada et al. indicated that proteasome inhibitors enhance the stability of certain ALDP mutants but did not increase peroxisomal β-oxidation in the corresponding cells [29]. While these results may seem contradictory to those reported here, it is important to

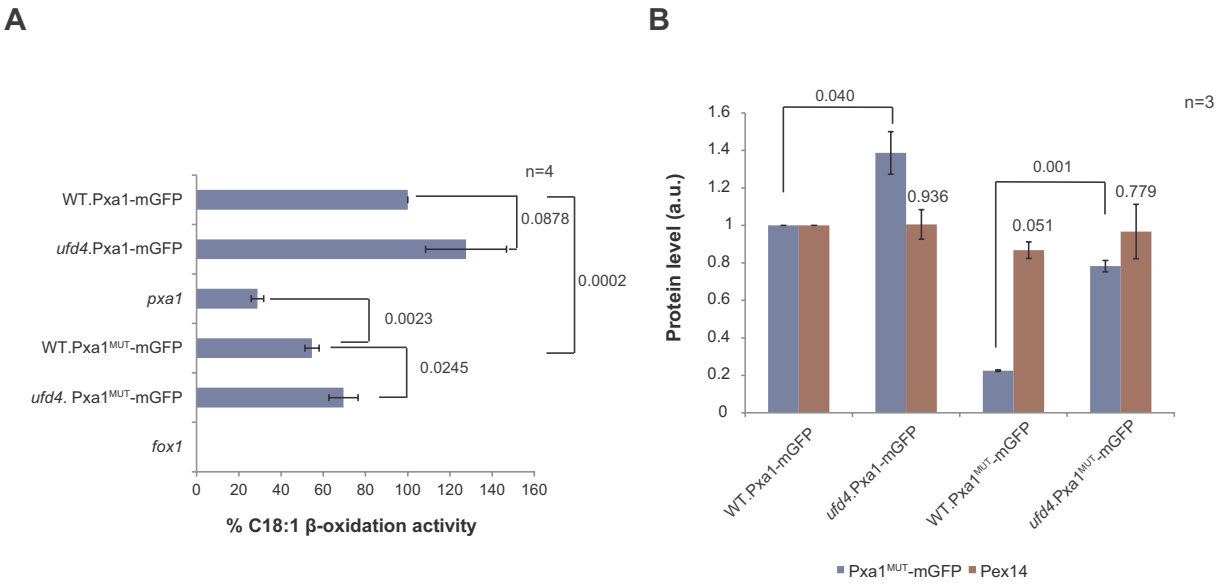

Fig. 7. Inhibiting Pxa1^{MUT}-mGFP degradation enhances β-oxidation activity *in vivo*.
A Bar chart displaying β-oxidation activity in WT and *ufd4* cells expressing Pxa1-mGFP or Pxa1^{MUT}-mGFP. β-oxidation activity was measured in cells grown overnight on oleate/glucose media. β-oxidation in *pxa1* and *fox1* cells acts as control. The activity in WT.Pxa1-mGFP cells was taken as a reference [100%]. Values represent the mean ± SD of four independent experiments. Numbers above the columns depict the p-value calculated to determine whether changes to β–oxidation activity in the different strains, are significant.
B Bar chart displaying Pxa1-mGFP and Pxa1^{MUT}-mGFP levels in WT and *ufd4* cells. Pex14p levels in WT and *ufd4* cells acts as a control. Cells pre-cultivated on glucose were grown on oleate/glucose to an OD_{600} of 1.5, cells were lysed and samples were probed by immunoblotting. For quantification, blots in Fig. S2C were used. Pxa1-mGFP levels in WT.Pxa1-mGFP cells were set to 1. Similarly, Pex14 levels in WT.Pxa1-mGFP cells were used as a reference and set to 1. Values represent the mean ± SD of three independent experiments. Numbers above the columns depict the p-value calculated to determine whether changes to Pxa1/Pxa1^{MUT}-mGFP or Pex14p levels in the different strains, when compared to the corresponding WT strain, are significant.

note that the location where the mutants build up upon stabilization is critical in determining whether stabilization will result in enhanced activity. Yamada and co-workers did not address this in their study [29] and it is possible that these ALDP mutants are stabilized elsewhere in the cell. Hence, further work on the mechanism of ALDP degradation is therefore needed to understand at which point blocking ALDP mutant degradation could positively affect ALDP activity. Nevertheless, our data demonstrate that *UFD4* deletion results in a build-up of Pxa1^{MUT}-mGFP at the peroxisomal membrane and significantly, a human homologue of Ufd4p, known as TRIP12 [70], is involved in the degradation of a range of different proteins [71–73]. It would therefore be interesting to investigate whether TRIP12 has a role in ALDP degradation and if so, whether blocking TRIP12 dependent ALDP mutant degradation improves β-oxidation in ALD patients.

In summary, we have demonstrated that a faulty peroxisomal fatty acid transporter undergoes proteasome-mediated degradation and identify Ufd4p as playing an important role in facilitating this degradation. In addition, these results may help to shed new light on the role of ALDP degradation in ALD.

4. Materials and methods

4.1. Construction of plasmids and S. cerevisiae strains

S. cerevisiae transformations were performed with the Lithium acetate method, as described previously [74]. *S. cerevisiae* strains and plasmids used in this study are listed in Tables 1 and 2 respectively. The primers used in the study are listed in Table S1. Phusion DNA polymerase (Thermo Scientific) was used for the amplification of gene fragments.

The *S. cerevisiae* WT.Pxa1-mGFP strain was constructed as follows. PCR was performed on pHIPZ-mGFP using the Pxa1-mGFP Fw and Pxa1-mGFP Rev. primers to amplify the C-terminal region of *PXA1* together with the Zeocin resistance cassette (*bleMX6*) and the mGFP coding sequences and the obtained PCR fragment was transformed into the yMaM330 strain. The plasmid pGW053 was constructed as follows: the genomic region of the *PXA1* gene was amplified by PCR using Forward primer VIP1080, 485 bp upstream of open reading frame and Reverse primer VIP1081, 192 bp downstream of ORF. This was inserted into Ycplac111 using gap repair between EcoR1 and *Hin*dIII sites, resulting in pGW046. This plasmid was used as template for site directed mutagenesis to generate Pxa1 G650S/K651R using VIP672 and VIP673, producing pGW053. For the construction of *S. cerevisiae* WT.Pxa1^{MUT}-mGFP, first a recombinant plasmid pHIPZ-Pxa1^{MUT}-mGFP was constructed. PCR was performed on pGW053 using Pxa1^{MUT} Fw and Pxa1^{MUT} Rev. primers to amplify the C-terminal region of *PXA1* (carrying the two mutations *G650S/K651R*) and to introduce PciI and *Bgl*II sites. The resulting DNA fragment, digested with PciI and BglII, was cloned into PciI/BglII cut pHIPZ-mGFP to generate pHIPZ-Pxa1^{MUT}-mGFP. PCR was then performed on pHIPZ-Pxa1^{MUT}-mGFP using Int_Pxa1^{MUT} Fw and Int_Pxa1^{MUT} Rev. to amplify the Pxa1^{MUT}-mGFP fragment and the obtained PCR product was then transformed into the yMaM330 strain. The obtained PCR fragment was also transformed into *pdr5*, *atg12* and *ufd4* strains to *pdr5*.Pxa1^{MUT}-mGFP, *atg12*.Pxa1^{MUT}-mGFP and *ufd4*.Pxa1^{MUT}-mGFP respectively. The positive transformants of WT.Pxa1^{MUT}-mGFP, *pdr5*.Pxa1^{MUT}-mGFP, *atg12*.Pxa1^{MUT}-mGFP and *ufd4*.Pxa1^{MUT}-mGFP were checked both by colony PCR and sequencing. In addition, PCR fragment was also transformed into *nam7*, *ela1*, *dsk2*, *skp2*, *dma2* and *tul1* cells to generate the mutant strains expressing Pxa1^{MUT}-mGFP.

The *S. cerevisiae* Pxa1-tFT strain was generated as follows. PCR was performed on pMaM168 to amplify C-terminal region of *PXA1* and tFT tagging module using primers Pxa1-tFT Fw and Pxa1-tFT Rev. The generated PCR product was then transformed into yMaM330. Strains expressing Pex3-mKate2 were constructed as follows. Pex3-mKate2 cassette consisting of C-terminal region of *PEX3*, hygromycin resistance gene (*hphMX*) and mKate2 coding sequences was amplified from pHIPH-Pex14mKate2 using primers Pex3-mKate Fw and Pex3-mKate

Table 1
Yeast strains used in this study.

Strain	Description [genotype]	Reference
BY4741	*MATa his3Δ1 leu2Δ0 met15Δ0 ura3Δ0*	[82] (Knop lab)
BJ1991	*MATa, leu2, trp1, ura3-251, prb1-1122, pep4-3, gal2*	[80]
yMaM330 [Wild type- WT]	*MATalpha his3Δ1 leu2Δ0 met15Δ0 ura3Δ0 can1Δ:: STE2pr-spHIS5 lyp1Δ::STE3pr-LEU2 leu2Δ::GAL1pr- I-SCEI-natNT2*	[82] (Knop lab)
WT.PEX3-mKate2	*yMaM330, PEX3::mKate2-hphMX*	This study (Fig. 1)
WT.PXA1-mGFP	*yMaM330, PXA1::mGFP-bleMX6*	This study (Figs. 1, 2, 4, 7, S1 and S2)
WT.PXA1^{MUT}-mGFP	*yMaM330, PXA1G650S/K651R::mGFP-bleMX6*	This study (Figs. 1, 2, 3, 4, 5, 6, 7, S1 and S2)
WT. PXA1^{MUT}-mGFP + PEX3-mKate2	*yMaM330, WT. PXA1^{MUT}-mGFP + PEX3::mKate2-hphMX*	This study (Fig. 1)
WT. PXA1-mGFP + PEX3-mKate2	*yMaM330, WT. PXA1-mGFP + PEX3::mKate2-hphMX*	This study (Fig. 1 and Fig. 2)
WT. PXA1^{MUT}-mGFP + DsRed-SKL	*yMaM330, WT. PXA1^{MUT}-mGFP + SKL::DsRed-hphMX*	This study (Fig. S1)
PXA1-tFT	*yMaM330, PXA1::mCherry-I-SceIsite-SpCYC1term-ScURA3-I-SceIsite-mCherryΔN-sfGFP*	This study (Figs. 4 and S1H)
PEX11-tFT	*yMaM330, PEX11::mCherry-I-SceIsite-SpCYC1term-ScURA3-I-SceIsite-mCherryΔN-sfGFP*	Knop lab (Figs. 4 and S1H)
UPS deletion library	*BY4741, goi deletions::kanMX*	[82]
yMaM344	*yMaM330, ura3Δ0::mCherryΔN-I-SceIsite-SpCYC1term-ScURA3-I-SceIsite-mCherryΔN*	[82]
atg12	*atg12 deletion strain, BY4741, atg12::kanMX*	Knop lab
pex2	*pex2 deletion strain, BY4741, pex2::kanMX*	Knop lab
pex4	*pex4 deletion strain, BY4741, pex4::kanMX*	Knop lab
ufd4	*ufd4 deletion strain, BY4741, ufd4::kanMX*	Knop lab
pdr5	*pdr5 deletion strain, BY4741, pdr5::kanMX*	Knop lab
nam7	*nam7 deletion strain, BY4741, nam7::kanMX*	Knop lab
ela1	*ela1 deletion strain, BY4741, ela1::kanMX*	Knop lab
dsk2	*dsk2 deletion strain, BY4741, dsk2::kanMX*	Knop lab
skp2	*skp2 deletion strain, BY4741, skp2::kanMX*	Knop lab
dma2	*dma2 deletion strain, BY4741, dma2::kanMX*	Knop lab
tul1	*tul1 deletion strain, BY4741, tul1::kanMX*	Knop lab
atg12.PXA1-tFT	*yMaM330, PXA1-tFT + atg12::kanMX*	This study (Fig. 4)
pex2.PXA1-tFT	*yMaM330, PXA1-tFT + pex2::kanMX*	This study (Fig. 4)
pex4.PXA1-tFT	*yMaM330, PXA1-tFT + pex4::kanMX*	This study (Fig. 4)
pdr5.PXA1^{MUT}-mGFP	*BY4741, pdr5 + PXA1G650S/K651R:: mGFP-bleMX6*	This study (Figs. 2 and S1)
atg12.PXA1^{MUT}-mGFP	*BY4741, atg12 + PXA1G650S/K651R:: mGFP-bleMX6*	This study (Figs. 2, 4, S1 and S2)
pex2.PXA1^{MUT}-mGFP	*YMaM330, WT. PXA1^{MUT}-mGFP + pex2 deletion pex2::kanMX*	This study (Figs. 5 and S2)
pex2.PXA1^{MUT}-mGFP + PEX3-mKate2	*yMaM330, pex2* PXA1^{MUT}-mGFP + *PEX3::mKate2-hphMX*	This study (Fig. 5)
pex4.PXA1^{MUT}-mGFP	*YMaM330, WT. PXA1^{MUT}-mGFP + pex4 deletion pex4::kanMX*	This study (Figs. 5 and S2)
pex4.PXA1^{MUT}-mGFP + PEX3-mKate2	*yMaM330, pex4* PXA1^{MUT}-mGFP + *PEX3::mKate2-hphMX*	This study (Fig. 5)
pex5.PXA1^{MUT}-mGFP	*YMaM330, WT. PXA1^{MUT}-mGFP + pex5 deletion pex5::kanMX*	This study (Figs. 5 and S2)
pex5.PXA1^{MUT}-mGFP + PEX3-mKate2	*yMaM330, pex5* PXA1^{MUT}-mGFP + *PEX3::mKate2-hphMX*	This study (Fig. 5)
ufd4.PXA1^{MUT}-mGFP	*BY4741, ufd4 + PXA1G650S/K651R::mGFP-bleMX6*	This study (Figs. 6, 7 and S2)
ufd4.PXA1^{MUT}-mGFP + PEX3-mKate2	*ufd4* PXA1^{MUT}-mGFP + *PEX3::mKate2-hphMX*	This study (Fig. 6)
nam7.PXA1^{MUT}-mGFP	*BY4741, nam7 + PXA1G650S/K651R::mGFP-bleMX6*	This study (Fig. 6)
ela1.PXA1^{MUT}-mGFP	*BY4741, ela1 + PXA1G650S/K651R::mGFP-bleMX6*	This study (Fig. 6)
dsk2.PXA1^{MUT}-mGFP	*BY4741, dsk2 + PXA1G650S/K651R::mGFP-bleMX6*	This study (Fig. 6)
skp2.PXA1^{MUT}-mGFP	*BY4741, skp2 + PXA1G650S/K651R::mGFP-bleMX6*	This study (Fig. 6)
dma2.PXA1^{MUT}-mGFP	*BY4741, dma2 + PXA1G650S/K651R::mGFP-bleMX6*	This study (Fig. 6)
tul1.PXA1^{MUT}-mGFP	*BY4741, tul1 + PXA1G650S/K651R::mGFP-bleMX6*	This study (Fig. 6)
ufd4.PXA1^{MUT}-mGFP + DsRed-SKL	*ufd4* PXA1^{MUT}-mGFP + *SKL::DsRed-hphMX*	This study (Fig. S1)
ufd4.PXA1-mGFP	*BY4741, ufd4 + PXA1::mGFP-bleMX6*	This study (Figs. 7 and S2)
fox1	*BJ1991, fox1::kanMX*	
pxa1	*yMaM330, pxa1 deletion, pxa1::hphMX*	This study (Fig. 7)
WT.PXA1^{MUT}-mGFP + MycUb^{K48R}	*yMaM330, WT PXA1^{MUT}-mGFP + P_{CUP1}-MycUbK48R* [*yeast episomal plasmid*, Y_{EP}-Pcup1-MycUbK48R]	This study (Figs. 3 and S1)
WT.PXA1^{MUT}-mGFP + MycUb	*WT PXA1^{MUT}-mGFP + P_{CUP1}-MycUb* [*yeast episomal plasmid*, Y_{EP}-Pcup1-MycUb]	This study (Figs. 3 and S1)
pdr5 + MycUb	*pdr5* + [*yeast episomal plasmid*, Y_{EP}-Pcup1-MycUb]	This study (Figs. 2 and S1)
pdr5.PXA1^{MUT}-mGFP + MycUb	*pdr5*.PXA1^{MUT}-mGFP + [*yeast episomal plasmid*, Y_{EP}-Pcup1-MycUb]	This study (Figs. 2 and S1)

Rev. The generated PCR fragment was transformed into WT, WT.Pxa1-mGFP, WT.Pxa1^{MUT}-mGFP and *ufd4*.Pxa1^{MUT}-mGFP. Furthermore, the PCR fragment was also transformed into *pex2*. Pxa1^{MUT}-mGFP, *pex4*. Pxa1^{MUT}-mGFP and *pex5*. Pxa1^{MUT}-mGFP strains, which were generated as described below.

S. cerevisiae WT.Pxa1^{MUT}-mGFP and *ufd4*.Pxa1^{MUT}-mGFP strains expressing DsRed-SKL were constructed as follows. First, the PCR cassette (consisting of *TEF* promoter and DsRed-SKL coding sequences) was digested *NotI/SalI* and cloned into NotI/SalI cut pHIPX7-DsRed-SKL to create pHIPH7-DsRed-SKL. The PCR cassette containing *TDH3* promoter sequence was amplified from pP_{TDH3}-GFP-SKL was digested with NotI/BamHI and cloned into NotI/BamHI cut pHIPH7-DsRed-SKL, to create pHIPH8-DsRed-SKL. The resulting plasmid after linearization with MunI was transformed into WT.Pxa1^{MUT}-mGFP and *ufd4*.Pxa1^{MUT}-mGFP strains to generate WT.Pxa1^{MUT}-mGFP. DsRedSKL and *ufd4*.Pxa1^{MUT}-mGFP. DsRed-SKL respectively. In these strains, the expression of DsRed-SKL was under the control of *TDH3* promoter.

S. cerevisiae WT.Pxa1^{MUT}-mGFP + MycUb and WT.Pxa1^{MUT}-mGFP + MycUbK48R strains were constructed as follows. First, the Yeast episomal plasmids (Y_{EP}) expressing MycUb and MycUbK48R from the CUP1 promoter were constructed: the *CUP1* promoter coding sequence was amplified from pCGCN-FAA4 using primers CUP1_Fw and CUP1_Rev, digested with NotI/BamHI and cloned into NotI/BamHI cut pRDV1 (MycUb) or pRDV2 (MycUbK48R). The resulting vectors were then used to amplify Pcup1-MycUb and Pcup1-MycUbK48R sequences individually using primers CUP1_Fw and MycUb/UbK48R_Rev and these PCR fragments were digested with NotI and *Sac*I and cloned into NotI/SacI cut pRG226 (Addgene, 64529). The Y_{EP}-P_{CUP1}-MycUbK48R plasmid was transformed into the WT.Pxa1^{MUT}-mGFP strain to generate WT.Pxa1^{MUT}-mGFP + MycUbK48R. The Y_{EP}-P_{CUP1}-MycUb plasmid was

Table 2
Plasmids used in this study.

Plasmid	Description	Use	Reference
pGW053	YCplac111 plasmid containing *PXA1* carrying two mutations *G650S/K651R*; *LEU2*, Amp^R	Amplification of C-terminal *PXA1* (with *G650S/K651R*)	This study
pHIPZ-mGFP fusinator	pHIPZ containing *mGFP*; *bleMX6*, Amp^R	1. Vector for cloning 2. C-terminal *mGFP* tagging to *PXA1*; genome integration	[83]
pHIPZ-Pxa1^{MUT}-mGFP	pHIPZ- *mGFP* containing C-terminal *PXA1* with two mutations G650S/K651R [$PXA1^{MUT}$]; *bleMX6*, Amp^R	C-terminal *mGFP* tagging to $PXA1^{MUT}$; genome integration	This study
pHIPH-Pex14mKate2	pHIPH containing *mKate2* and C-terminal of *PEX14*; *hphMX*, Amp^R	1. C-terminal *mKate2* tagging to *PEX3*; genome integration 2. Gene disruption (*pxa1*) by *hphMX* marker	[9]
pFA6a- kanMX6	pFA6a plasmid containing geneticin (*kanMX6*) resistance gene; *kanMX*, Amp^R	Gene disruption (*atg12*, *pex2*, *pex4 and pex5*) by *kanMX6* marker	[82]
pMaM168	pFA6a plasmid containing tFT module (*mCherry-I-SceIsite-SpCYC1term-ScURA3-I-SceIsite-mCherryΔN-sfGFP*); *URA3*, Amp^R	1. C-terminal *tFT* tagging; *PXA1-tFT* and *PEX11-tFT* integration into yMaM330	[82]
pRG226	Yeast episomal plasmid (Y_{EP}); *URA3*, 2 μ ori	Vector for cloning	Addgene, 64529
pCGCN-FAA4	Plasmid containing *CUP1* promoter and *mGFP*; *bleMX6*, Amp^R	Amplification of *CUP1* promoter; cloning	[83]
pRDV1	Plasmid containing *Myc* tagged ubiquitin (*Ub*) under control of *DHAS* promoter; *hphMX*, Amp^R	Amplification of *MycUb*; vector for cloning	[10]
pRDV2	Plasmid containing *Myc* tagged ubiquitin mutant (*UbK48R*) under the control of *DHAS* promoter; *hphMX*, Amp^R	Amplification of *MycUbK48R*; Vector for cloning	[10]
Y_{EP}-P_{CUP1}-MycUb	Yeast episomal plasmid (Y_{EP}) containing *CUP1p*romoter and *MycUb*; *URA3*, Amp^R	Integration into WT. $PXA1^{MUT}$-*mGFP* strain	This study
Y_{EP}-P_{CUP1}-MycUbK48R	Yeast episomal plasmid (Y_{EP}) containing *CUP1promoter* and *MycUbK48R*; *URA3*, Amp^R	Integration into WT and WT. $PXA1^{MUT}$-*mGFP*	This study
pHIPX7-DsRedSKL	Plasmid containing DsRed-SKL under the control of *TEF* promoter; *LEU2*, Amp^R	Vector for cloning	[84]
pHIPH7-DsRed-SKL	Plasmid containing DsRed-SKL under the control of *TEF* promoter; *hphMX*, kan^R	Vector for cloning	This study
pP_{TDH3}-GFP-SKL	Plasmid containing GFP-SKL under the control of *TDH3* promoter; *LEU2*, Amp^R	Amplification of *TDH3* promoter; cloning	[85]
pHIPH8-DsRedSKL	Plasmid containing DsRed-SKL under the control of *TDH3* promoter, *hphMX* Amp^R	Integration into WT. $PXA1^{MUT}$-*mGFP* and *ufd4*. $PXA1^{MUT}$-*mGFP* strain	This study

transformed individually into WT.Pxa1^{MUT}-mGFP, *pdr5*.Pxa1^{MUT}-mGFP and *pdr5* strains to generate WT.Pxa1^{MUT}-mGFP + MycUb, *pdr5*.Pxa1^{MUT}-mGFP + MycUb and *pdr5* + MycUb respectively.

4.2. Construction of S. cerevisiae deletion strains

The *pxa1* deletion strain was constructed by replacing the *PXA1* region with the hygromycin resistance gene (*hphMX*). A PCR fragment containing the hygromycin resistance gene and *PXA1* flanking regions were amplified from pHIPH-Pex14mKate2 using primers DPxa1_Fw and DPxa1_Rev. The resulting *PXA1* deletion cassette was transformed into yMaM330. For the construction of *pex5*.Pxa1^{MUT}-mGFP, the *PEX5* deletion cassette (geneticin resistance gene and *PEX5* flanking regions) amplified from pFa6AkanMX6 using primers DPex5_Fw and DPex5_Rev was transformed in WT.Pxa1^{MUT}-mGFP.

S. cerevisiae pex2 and *pex4* strains expressing Pxa1^{MUT}-mGFP or Pxa1-tFT were constructed as follows. The *pex2* and *pex4* deletion cassettes consisting of geneticin resistance cassette (*kanMX*) and *PEX2* or *PEX4* flanking regions were amplified from pFa6AkanMX6 using DPex2_Fw and DPex2_Rev (for *PEX2* deletion cassette) and DPex4_Fw and DPex4_Rev (for *PEX4* deletion cassette). The obtained deletion cassettes were then transformed individually into WT.Pxa1^{MUT}-mGFP and Pxa1-tFT strains to generate *pex2*. Pxa1^{MUT}-mGFP, *pex4*. Pxa1^{MUT}-mGFP, *pex2*.Pxa1-tFT and *pex4*.Pxa1-tFT strains.

For the construction of *atg12*.Pxa1-tFT strain, deletion cassette consisting of geneticin resistance cassette (*kanMX*) and *ATG12* flanking regions was amplified from pFa6AkanMX6 using primers DAtg12_Fw and DAtg12_Rev (for *ATG12* deletion cassette). The obtained deletion cassette was then transformed into Pxa1-tFT to generate *atg12*.Pxa1-tFT strain.

All gene integrations were confirmed by colony PCR using Phire Hot Start II DNA polymerase (Thermo Fisher Scientific) and gene deletions were checked by colony PCR as well as southern blotting analysis of chromosomal DNA, using the ECL Direct Nucleic Acid Labelling and Detection system (Thermo Fisher Scientific), according to the protocol provided by the manufacturer.

4.3. Growth conditions

The *Escherichia coli* strain DH5α was used for cloning purposes. *E. coli* cells were grown in LB supplemented with 100 μg/mL Ampicillin at 37 °C. Yeast transformants were selected on YPD plates containing 2% agar and 100 μg/mL Zeocin (Invitrogen), 150 μg/mL Geneticin (Invitrogen) or 300 μg/mL Hygromycin (Invitrogen) or on YND plates containing 6.7 g/L yeast nitrogen base without amino acids (YNB, Difco), 5 g/L D- glucose monohydrate (Sigma-Aldrich), 2% agar and 30 mg/L Leucine, 20 mg/L Histidine and 20 mg/L Methionine or 30 mg/L Uracil, when required.

For all the experiments, yeast cells were initially cultured at 30 °C on YM2 medium (6.7 g/L YNB, 1% casein hydrolysate (Sigma-Aldrich), 60 mg/L uracil, 60 mg/L tryptophan) containing either 2% or 0.3% (w/v) glucose. To induce peroxisome proliferation, cells grown on YM2 medium plus 0.3% glucose were transferred to YNO-glucose medium (6.7 g/L YNB, 1% casein hydrolysate, 60 mg/L uracil, 60 mg/L tryptophan, 0.05% tween, 0.1% oleate and 0.1% glucose). For strains expressing Myc tagged ubiquitin: MycUb and MycUb^{K48R} under the control of *CUP1* promoter and uracil coding gene, *URA3* (Table 1), cells were pre-cultured at 30 °C on YM2 medium (lacking uracil) plus 0.3% glucose and then grown on YNO-glucose medium (lacking uracil) to an OD_{600} of 1.5. To inhibit protein synthesis, cells were treated with cycloheximide (CHX, Sigma-Aldrich) to a final concentration of 6 mg/mL. To inhibit proteasome, cells were treated with 70 μM of MG1232 (Sigma-Aldrich) and 70 μM of Bortezomib (Selleckchem).Where indicated, an equal amount of DMSO (control for CHX) was added to cells. For spot assays, yeast strains were grown overnight on YM2 medium containing 2% glucose and shifted to YM2 medium plus 0.3%

glucose. After 6 h of growth in YM2 plus 0.3 glucose, yeast cells were spotted onto oleate plates containing 6.7 g/L YNB, 0.1% yeast extract, 0.1% oleate, 0.05% Tween, 2% agar and when required uracil (30 mg/L), leucine (60 mg/L), methionine (20 mg/L) and histidine (20 mg/L) was added. Plates were incubated at 30 °C for 7 days before imaging.

4.4. Preparation of yeast TCA lysates

Cell extracts of TCA-treated cells were prepared for SDS-PAGE as described previously [75]. SDS-PAGE and western blotting were performed by established methods. Equal volume of samples were loaded per lane and blots were probed with antibodies against mGFP (Santa Cruz Biotech, sc-9996), pyruvate carboxylase 1 (Pyc), Pex14p, rabbit polyclonal antisera raised against the Myc tag (Santa Cruz Biotech, sc-789) or HA tag (Sigma, H6908). Secondary goat anti-rabbit (Thermo Fisher Scientific, 31460) or goat anti-mouse (Thermo Fisher Scientific, 31430) antibodies conjugated to horseradish peroxidase or alkaline phosphatase were used for detection. Pyc was used as a loading control.

4.5. Quantification of Western blots

Western blots were scanned using a densitometer (Bio-Rad, GS-710) and protein levels were quantified using Image J software (https://imagej.nih.gov/ij/). The intensity of each band measured was normalized by dividing by the intensity of the corresponding Pyc band (loading control). The normalized Pxa1^{MUT}-mGFP values were compared to Pxa1-mGFP values, which was set to 1. The levels of Pxa1^{MUT}-mGFP in mutant cells are displayed relative to Pxa1^{MUT}-mGFP levels in WT (set to 1). For CHX experiments, the normalized values at time point 0 (T0) was set to 1.0 and values obtained after CHX addition at indicated time points are displayed as a fraction of T0 values. Standard deviations were calculated using Excel. Significance was determined using two tailed student's *t*-test. * represents *P*-values < 0.05, ** represents P-values < 0.01, and *** represents P-values < 0.001. The data presented are derived from three independent experiments.

4.6. tFT screening with UPS deletion library

Tandem fluorescent protein timers (tFT): mCherry and sfGFP were endogenously tagged to Pxa1 as described [76]. By the use of a pinning robot (Singer Instruments), Pxa1-tFT was crossed to UPS deletion library or an array of haploid strains consisting of knockout, temperature sensitive (*ts*) and Decreased Abundance by mRNA perturbation (DAmp) alleles of individual components of the Ubiquitin Proteasome System (UPS) [44,77,78]. In addition, Pxa1-tFT was crossed to a control strain expressing *kanMX* selection marker from the *ura3*Δ locus, referred to as wild-type (WT). Screens were performed in 1536 format, with four technical replicates of each cross arranged next to each other. The selection of diploids, sporulation and the selection of haploids carrying Pxa1-tFT and a genetic perturbation, was performed by sequential pinning on appropriate selective media as described [79], followed by seamless marker excision [76]. Using an Infinite M1000 Pro plate reader equipped with automatic plate loading stacker (Tecan) and custom temperature control chamber, mCherry intensity (587/10 nm excitation, 610/10 nm emission) and sfGFP intensity (488/10 nm excitation, 510/10 nm emission) was measured from colonies grown on a modified YNO-glucose medium containing (6.7 g/L YNB, 2 g/L amino acid dropout mix (-LEU), 0.05% tween, 0.1% oleate, 0.1% glucose and 2% agar). First set of measurements were taken after 24 h of growth and measurements were taken every 24 h until 72 h (3 days).

Whole colony fluorescence intensities (mCherry and sfGFP), obtained from UPS mutant crossed to Pxa1-tFT, were corrected for auto fluorescence by subtracting the measurements of a corresponding mutant crossed to the control strain, yMaM344 (expressing non-fluorescent protein). The median value was calculated out of the four technical replicates. The corrected values of mCherry divided by the sfGFP values yielded a ratio, representing the stability of Pxa1-tFT in the UPS mutants. Similarly, the mCherry/sfGFP ratio of Pxa1-tFT in WT was corrected for auto fluorescence. Using the ratios obtained on day one, two and three a *Z*- score for each day was calculated by the formula. A Z-score indicates how many standard deviations a value is from the mean of all values. Z-score can be calculated from the formula: $Z = (X - \mu)/\sigma$. In the formula, Z is the Z-score, X is the value of the element, μ is the population mean, and σ is the standard deviation. A negative Z-score indicates that the value of the element is below average while positive Z-score indicates the value is above average. To identify UPS mutants which potentially increased the stability of Pxa1-tFT, Z-score (**Z**) was calculated using the formula.

$$\frac{Z = \text{mCherry / sfGFP ratio in a UPS mutant}(\mathbf{X}) - \text{mean mCherry / sfGFP ratio in WT and UPS mutants}(\boldsymbol{\mu})}{\text{Standard deviation of mCherry / sfGFP ratio in WT and UPS mutants}(\sigma)}$$

A strain (UPS mutant) with a Z-score of 0 indicates that Pxa1-tFT stability is similar to the WT as well to the population mean (WT and UPS mutants). While, the mutants with Z-score of 1.0 and 2.0 indicates that the mCherry/sfGFP ratio in a corresponding mutant is different from the WT and population mean by 1.0 and 2.0 standard deviations. Hence, mutant stains displaying a Z-score > 0 indicate enhanced Pxa1-tFT stability. UPS mutants with an increase in Z-score > 1.0 on two of the three days tested were considered as potential candidates that significantly increased Pxa1-tFT stability. The heat map generated using the Z-scores (obtained from mCherry/sfGFP ratio of Pxa1-tFT in UPS mutants and the WT) is presented in Fig. 2D.

4.7. Fluorescence microscopy

All images were captured at room temperature using an inverted microscope (Axio Scope A1, 100 × 1.30 NA Plan-Neofluar objective, Carl Zeiss), Micro-Manager software and a digital camera (CoolSNAP HQ^2; Photometrics). For wide field microscopy, GFP fluorescence was visualized with a 470/440-nm band pass excitation filter, a 495-nm dichromatic mirror, and 525/50-nm band pass emission filter. mCherry fluorescence was visualized with a 587/25-nm band pass excitation filter, a 605-nm dichromatic mirror, and 647/70-nm band pass emission filter.

For co-localization analysis, cells were pre-grown on YM2 medium containing glucose, transferred to YNO-glucose (low fluorescence) medium and grown until an OD_{600} of 1.5 after which fluorescence microscopy images were captured. For CHX chase analysis, cells grown in the same way as indicated above were treated with cycloheximide (CHX) and images were taken from cells grown on oleate/glucose at indicated time points (min) after CHX treatment (Fig. 2B). The acquired images were processed using Image J software (https://imagej.nih.gov/ij/) with optimal settings: mGFP (200, 500), mKate2 (200, 600) and DsRed (200, 500). For co-localization analysis in WT, *pex2*, *pex4* and *pex5* cells expressing Pxa1^{MUT}-mGFP and Pex3-mKate2 (Fig. 5C), images were processed using optimal settings: mGFP (200, 800) and mKate2 (200, 600). For quantifying the co-localization of Pxa1-mGFP or Pxa1^{MUT}-mGFP in cells expressing peroxisomal markers (Pex3-mKate2 or DsRed-SKL) (Figs. 1, 2, 6 and S1), a line was drawn along GFP and mKate2/DsRed-SKL spots using ImageJ and the intensity was measured. Using this data, normalized fluorescent intensity of green and red spots were calculated and plotted against the distance of the line (from the beginning to the end).

For quantification of the Pex3-mKate2 and Pxa1-mGFP or Pxa1^{MUT}-mGFP fluorescence intensities in CHX treated cells (Fig. 2C), a rectangular area was drawn using ImageJ to envelope the region containing the mGFP/mKate2 spot and pixel intensity inside the area was measured. Since the cells expressing Pxa1^{MUT}-mGFP contain very few mGFP positive spots at the later time points of CHX treatment, the rectangular area selected contained the peroxisomal marker or Pex3-mKate2 spots and the corresponding mGFP intensity was measured. The maximum fluorescence intensity of mGFP measured on peroxisomes was corrected

for the background intensity and a box plot was made using Microsoft Excel. The box represents values from the 25 percentile to the 75 percentile; the horizontal line through the box represents the median value. Whiskers indicate maximum and minimum values. The mKate2 intensity was calculated and displayed in a similar way (Fig. 2C). To calculate the mGFP/mKate2 intensity ratio, the maximum intensity of Pxa1-mGFP or Pxa1^{MUT}-mGFP, obtained at different time points after CHX treatment, was divided by the corresponding maximum intensity of Pex3-mKate2 in each cell. The dataset was subjected to the two-tail *t*-test. * represents *P*-values < 0.05, ** represents P-values < 0.01 and *** represents P-values < 0.001.

4.8. Immunoprecipitation assay

Immunoprecipitation was performed on cells grown on YNO-glucose medium for 10 h and incubated with proteasome inhibitors (MG132 and Bortezomib) for 90 min. Around 14 OD units of each strain were harvested by centrifugation. Immunoprecipitation using GFP-Trap® _M beads was performed according to manufacturer's protocol (Chromotek) with slight modifications. Cells were washed once with 1 mL cold lysis or RIPA buffer (50 mM Tris/Cl pH 7.5, 150 mM NaCl, 2 mM EDTA, 0.1% SDS, 1% Triton X-100 and 0.5% Deoxycholate) and resuspended in 0.75 mL of lysis buffer containing 2.5 μg/mL leupeptin and 1 mM PMSF (added just prior to use). Yeast cells were then lysed using glass beads (~30 min) and samples were centrifuged at 8000 rpm at 4 °C for 10 min to remove cellular debris and unbroken cells. A fraction of supernatant (Load fraction) was collected and stored for SDS-PAGE analysis. The remaining supernatant fractions were then incubated with 30 μl GFP-Trap® _M beads (Chromotek) for 2 h at 4 °C under constant mixing. The beads were magnetically separated until the supernatant was clear. The supernatant was discarded and beads were washed five times using 500 μl ice cold wash buffer (50 mM Tris/Cl pH 7.5, 150 mM NaCl and 2 mM EDTA). The GFP-Trap® _M beads were then resuspended in 60 μl 4× SDS-Sample buffer and boiled for 10 min at 95 °C. Finally, the beads were separated magnetically and the supernatant (Elute fraction) was collected. The load and elute fractions were subjected to SDS-PAGE and immunoblotting with antibodies against GFP and Myc tagged epitope.

4.9. β- Oxidation assay

Yeast strains were grown on glucose medium containing 5 g/L D glucose, and 6.7 g/L YNB. When required; histidine, leucine, uracil, or methionine was added. To induce peroxisome proliferation cells were grown for at least 24 h on 5 g/L glucose medium, and then transferred to YPO medium (1.07 g/L oleate, 2.16 g/L Tween-80, 5 g/L peptone, 3 g/L yeast extract, 25 mM potassium phosphate buffer (pH = 6)). Cells were grown overnight in YPO medium to induce β-oxidation. β-Oxidation assay in intact cells were performed as described previously by [80] with slight modifications. The β-oxidation capacity was measured in 50 mM MES, pH 6.0 and 9 g/L NaCl supplemented with 10 μM 1-^{14}C-oleate. Subsequently, ^{14}C-CO2 was trapped with 2 M NaOH and used to quantify the rate of fatty acid oxidation. Results are presented as percentages relative to the rate of oxidation of wild-type cells expressing Pxa1-mGFP (set to 100). The data presented are from four independent experiments and significance is calculated using two-tailed student's *t*-test. * represents P-values < 0.05, ** represents P-values < 0.01, and *** represents P-values < 0.001.

Supplementary data to this article can be found online at https://doi.org/10.1016/j.bbamem.2020.183342.

Declaration of competing interest

The authors declare that they have no known competing financial interests or personal relationships that could have appeared to influence the work reported in this paper.

Acknowledgments

The authors thank Alwin Slagter for assistance in strain construction, Daniel Kirrmaier for help with constructing the 'UPS library', Arjen Krikken for advice with processing of fluorescence microscopy images and Peter van Haastert and Maarten Linskens for critically reading the manuscript. This work was funded by a VIDI Fellowship (723.013.004) from the Netherlands Organisation for Scientific Research (NWO), awarded to CW. The visit of SD to the Knop lab was supported from the collaborative research centre grant SFB1036 from the German Research foundation.

Author's contributions

CW conceived and supervised the project, with input from EH, SK and MK. CW, SD, MM, CVR and XC designed the experiments. SD and CW analysed the data with the help from other authors. SD performed biochemical and fluorescence microscopy experiments with the support from XC. SD and MM performed tFT screening experiments. CVR performed β-oxidation experiment. EH was involved in plasmid construction, SD and CW wrote the manuscript with the contribution from all the authors.

References

[1] T. Gabaldon, Peroxisome diversity and evolution, Philos. Trans. R. Soc. Lond. Ser. B Biol. Sci. 365 (2010) 765–773.
[2] J.J. Smith, J.D. Aitchison, Peroxisomes take shape, Nat. Rev. Mol. Cell Biol. 14 (2013) 803–817.
[3] S. Kemp, I.C. Huffnagel, G.E. Linthorst, R.J. Wanders, M. Engelen, Adrenoleukodystrophy - neuroendocrine pathogenesis and redefinition of natural history, Nat. Rev. Endocrinol. 12 (2016) 606–615.
[4] J.M. Nuttall, A. Motley, E.H. Hettema, Peroxisome biogenesis: recent advances, Curr. Opin. Cell Biol. 23 (2011) 421–426.
[5] P.U. Mayerhofer, Targeting and insertion of peroxisomal membrane proteins: ER trafficking versus direct delivery to peroxisomes, Biochim. Biophys. Acta 1863 (2016) 870–880.
[6] Y. Fang, J.C. Morrell, J.M. Jones, S.J. Gould, PEX3 functions as a PEX19 docking factor in the import of class I peroxisomal membrane proteins, J. Cell Biol. 164 (2004) 863–875.
[7] C. Williams, L. Opalinski, C. Landgraf, J. Costello, M. Schrader, A.M. Krikken, et al., The membrane remodeling protein Pex11p activates the GTPase Dnm1p during peroxisomal fission, Proc. Natl. Acad. Sci. 112 (2015) 6377–6382.
[8] C.W. van Roermund, L. Ijlst, W. Majczak, H.R. Waterham, H. Folkerts, R.J. Wanders, et al., Peroxisomal fatty acid uptake mechanism in Saccharomyces cerevisiae, J. Biol. Chem. 287 (2012) 20144–20153.
[9] X. Chen, S. Devarajan, N. Danda, C. Williams, Insights into the role of the peroxisomal ubiquitination machinery in Pex13p degradation in the yeast Hansenula polymorpha, J. Mol. Biol. 430 (2018) 1545–1558.
[10] C. Williams, I.J. van der Klei, Pexophagy-linked degradation of the peroxisomal membrane protein Pex3p involves the ubiquitin-proteasome system, Biochem. Biophys. Res. Commun. 438 (2013) 395–401.
[11] J.S. Bett, Proteostasis regulation by the ubiquitin system, Essays Biochem. 60 (2016) 143–151.
[12] Y.H. Ye, M. Rape, Building ubiquitin chains: E2 enzymes at work, Nat. Rev. Mol. Cell Biol. 10 (2009) 755–764.
[13] B.A. Schulman, J.W. Harper, Ubiquitin-like protein activation by E1 enzymes: the apex for downstream signalling pathways, Nat. Rev. Mol. Cell Biol. 10 (2009) 319–331.
[14] M.B. Metzger, A.M. Weissman, Working on a chain: E3s ganging up for ubiquitylation, Nat. Cell Biol. 12 (2010) 1124–1126.
[15] J. Weber, S. Polo, E. Maspero, HECT E3 ligases: a tale with multiple facets, Front. Physiol. 10 (2019).
[16] M.B. Metzger, V.A. Hristova, A.M. Weissman, HECT and RING finger families of E3 ubiquitin ligases at a glance, J. Cell Sci. 125 (2012) 531–537.
[17] M.B. Metzger, J.N. Pruneda, R.E. Klevit, A.M. Weissman, RING-type E3 ligases: master manipulators of E2 ubiquitin-conjugating enzymes and ubiquitination, Bba-Mol Cell Res 1843 (2014) 47–60.
[18] R.J. Deshaies, C.A.P. Joazeiro, RING Domain E3 Ubiquitin Ligases, Annu. Rev. Biochem. 78 (2009) 399–434.
[19] D.M. Wenzel, A. Lissounov, P.S. Brzovic, R.E. Klevit, UBCH7 reactivity profile reveals parkin and HHARI to be RING/HECT hybrids, Nature 474 (2011) 105–U36.
[20] K.K. Dove, B. Stieglitz, E.D. Duncan, K. Rittinger, R.E. Klevit, Molecular insights into RBR E3 ligase ubiquitin transfer mechanisms, EMBO Rep. 17 (2016) 1221–1235.

[21] M. Schrader, H.D. Fahimi, Peroxisomes and oxidative stress, Biochim. Biophys. Acta 1763 (2006) 1755–1766.
[22] V. Costa, A. Quintanilha, P. Moradas-Ferreira, Protein oxidation, repair mechanisms and proteolysis in Saccharomyces cerevisiae, IUBMB Life 59 (2007) 293–298.
[23] N. Shani, A. Sapag, P.A. Watkins, D. Valle, An S. cerevisiae peroxisomal transporter, orthologous to the human adrenoleukodystrophy protein, appears to be a heterodimer of two half ABC transporters: Pxa1p and Pxa2p, Ann. N. Y. Acad. Sci. 804 (1996) 770–772.
[24] E.H. Hettema, C.W. van Roermund, B. Distel, M. van den Berg, C. Vilela, C. Rodrigues-Pousada, et al., The ABC transporter proteins Pat1 and Pat2 are required for import of long-chain fatty acids into peroxisomes of Saccharomyces cerevisiae, EMBO J. 15 (1996) 3813–3822.
[25] N. Shani, P.A. Watkins, D. Valle, PXA1, a possible Saccharomyces cerevisiae ortholog of the human adrenoleukodystrophy gene, Proc. Natl. Acad. Sci. U. S. A. 92 (1995) 6012–6016.
[26] M. Engelen, S. Kemp, B.T. Poll-The, X-linked adrenoleukodystrophy: pathogenesis and treatment, Curr. Neurol. Neurosci Rep. 14 (2014) 486.
[27] M. Morita, S. Matsumoto, A. Sato, K. Inoue, D.G. Kostsin, K. Yamazaki, et al., Stability of the ABCD1 protein with a missense mutation: a novel approach to finding therapeutic compounds for X-linked adrenoleukodystrophy, JIMD Rep. 44 (2019) 23–31.
[28] X. Zhang, C. De Marcos Lousa, N. Schutte-Lensink, R. Ofman, R.J. Wanders, S.A. Baldwin, et al., Conservation of targeting but divergence in function and quality control of peroxisomal ABC transporters: an analysis using cross-kingdom expression, Biochem. J. 436 (2011) 547–557.
[29] T. Yamada, N. Shinnoh, T. Kobayashi, Protease inhibitors suppress the degradation of mutant adrenoleukodystrophy proteins but do not correct impairment of very long chain fatty acid metabolism in adrenoleukodystrophy fibroblasts, Neurochem. Res. 22 (1997) 233–237.
[30] N. Takahashi, M. Morita, T. Maeda, Y. Harayama, N. Shimozawa, Y. Suzuki, et al., Adrenoleukodystrophy: subcellular localization and degradation of adrenoleukodystrophy protein (ALDP/ABCD1) with naturally occurring missense mutations, J. Neurochem. 101 (2007) 1632–1643.
[31] V. Feigenbaum, G. Lombard-Platet, S. Guidoux, C.O. Sarde, J.L. Mandel, P. Aubourg, Mutational and protein analysis of patients and heterozygous women with X-linked adrenoleukodystrophy, Am. J. Hum. Genet. 58 (1996) 1135–1144.
[32] P. Roerig, P. Mayerhofer, A. Holzinger, J. Gartner, Characterization and functional analysis of the nucleotide binding fold in human peroxisomal ATP binding cassette transporters, FEBS Lett. 492 (2001) 66–72.
[33] A. Gurvitz, H. Rottensteiner, The biochemistry of oleate induction: transcriptional upregulation and peroxisome proliferation, Biochim. Biophys. Acta 1763 (2006) 1392–1402.
[34] I.V. Karpichev, G.M. Small, Global regulatory functions of Oaf1p and Pip2p (Oaf2p), transcription factors that regulate genes encoding peroxisomal proteins in Saccharomyces cerevisiae, Mol. Cell. Biol. 18 (1998) 6560–6570.
[35] J.J. Smith, M. Marelli, R.H. Christmas, F.J. Vizeacoumar, D.J. Dilworth, T. Ideker, et al., Transcriptome profiling to identify genes involved in peroxisome assembly and function, J. Cell Biol. 158 (2002) 259–271.
[36] J. Golin, S.V. Ambudkar, L. May, The yeast Pdr5p multidrug transporter: how does it recognize so many substrates? Biochem. Biophys. Res. Commun. 356 (2007) 1–5.
[37] J.A. Fleming, E.S. Lightcap, S. Sadis, V. Thoroddsen, C.E. Bulawa, R.K. Blackman, Complementary whole-genome technologies reveal the cellular response to proteasome inhibition by PS-341, Proc. Natl. Acad. Sci. U. S. A. 99 (2002) 1461–1466.
[38] V. Dederer, A. Khmelinskii, A.G. Huhn, V. Okreglak, M. Knop, M.K. Lemberg, Cooperation of mitochondrial and ER factors in quality control of tail-anchored proteins, eLife 8 (2019).
[39] T. Hanada, N.N. Noda, Y. Satomi, Y. Ichimura, Y. Fujioka, T. Takao, et al., The Atg12-Atg5 conjugate has a novel E3-like activity for protein lipidation in autophagy, J. Biol. Chem. 282 (2007) 37298–37302.
[40] J.S. Thrower, L. Hoffman, M. Rechsteiner, C.M. Pickart, Recognition of the polyubiquitin proteolytic signal, EMBO J. 19 (2000) 94–102.
[41] A. Khmelinskii, P.J. Keller, A. Bartosik, M. Meurer, J.D. Barry, B.R. Mardin, et al., Tandem fluorescent protein timers for in vivo analysis of protein dynamics, Nat. Biotechnol. 30 (2012) 708–714.
[42] A. Khmelinskii, M. Meurer, C.T. Ho, B. Besenbeck, J. Fuller, M.K. Lemberg, et al., Incomplete proteasomal degradation of green fluorescent proteins in the context of tandem fluorescent protein timers, Mol. Biol. Cell 27 (2016) 360–370.
[43] A.H. Tong, C. Boone, Synthetic genetic array analysis in Saccharomyces cerevisiae, Methods Mol. Biol. 313 (2006) 171–192.
[44] M. Schuldiner, S.R. Collins, N.J. Thompson, V. Denic, A. Bhamidipati, T. Punna, et al., Exploration of the function and organization of the yeast early secretory pathway through an epistatic miniarray profile, Cell 123 (2005) 507–519.
[45] B. Agne, N.M. Meindl, K. Niederhoff, H. Einwachter, P. Rehling, A. Sickmann, et al., Pex8p: an intraperoxisomal organizer of the peroxisomal import machinery, Mol. Cell 11 (2003) 635–646.
[46] G. Sargent, T. van Zutphen, T. Shatseva, L. Zhang, V. Di Giovanni, R. Bandsma, et al., PEX2 is the E3 ubiquitin ligase required for pexophagy during starvation, J. Cell Biol. 214 (2016) 677–690.
[47] S.E. Burkhart, Y.T. Kao, B. Bartel, Peroxisomal ubiquitin-protein ligases peroxin2 and peroxin10 have distinct but synergistic roles in matrix protein import and peroxin5 retrotranslocation in Arabidopsis, Plant Physiol. 166 (2014) 1329–1344.
[48] I. Van der Leij, M.M. Franse, Y. Elgersma, B. Distel, H.F. Tabak, PAS10 is a tetratricopeptide-repeat protein that is essential for the import of most matrix proteins into peroxisomes of Saccharomyces cerevisiae, Proc. Natl. Acad. Sci. U. S. A. 90 (1993) 11782–11786.
[49] M.A. Theodoraki, N.B. Nillegoda, J. Saini, A.J. Caplan, A network of ubiquitin ligases is important for the dynamics of misfolded protein aggregates in yeast, J. Biol. Chem. 287 (2012) 23911–23922.
[50] S. Kemp, A. Pujol, H.R. Waterham, B.M. van Geel, C.D. Boehm, G.V. Raymond, et al., ABCD1 mutations and the X-linked adrenoleukodystrophy mutation database: role in diagnosis and clinical correlations, Hum. Mutat. 18 (2001) 499–515.
[51] J.E. Walker, M. Saraste, M.J. Runswick, N.J. Gay, Distantly related sequences in the alpha- and beta-subunits of ATP synthase, myosin, kinases and other ATP-requiring enzymes and a common nucleotide binding fold, EMBO J. 1 (1982) 945–951.
[52] L. Byeon, Z. Shi, M.D. Tsai, Mechanism of adenylate kinase. The “essential lysine” helps to orient the phosphates and the active site residues to proper conformations, Biochemistry 34 (1995) 3172–3182.
[53] E. Schneider, S. Wilken, R. Schmid, Nucleotide-induced conformational changes of MalK, a bacterial ATP binding cassette transporter protein, J. Biol. Chem. 269 (1994) 20456–20461.
[54] M.E. Zoghbi, G.A. Altenberg, ATP binding to two sites is necessary for dimerization of nucleotide-binding domains of ABC proteins, Biochem. Biophys. Res. Commun. 443 (2014) 97–102.
[55] N. Shani, D. Valle, A Saccharomyces cerevisiae homolog of the human adrenoleukodystrophy transporter is a heterodimer of two half ATP-binding cassette transporters, Proc. Natl. Acad. Sci. U. S. A. 93 (1996) 11901–11906.
[56] Y. Dang, L.M. Siew, Y.H. Zheng, APOBEC3G is degraded by the proteasomal pathway in a vif-dependent manner without being polyubiquitylated, J. Biol. Chem. 283 (2008) 13124–13131.
[57] S. Prakash, T. Inobe, A.J. Hatch, A. Matouschek, Substrate selection by the proteasome during degradation of protein complexes, Nat. Chem. Biol. 5 (2009) 29–36.
[58] S.L. Gonzalez, M. Stremlau, X. He, J.R. Basile, K. Munger, Degradation of the retinoblastoma tumor suppressor by the human papillomavirus type 16 E7 oncoprotein is important for functional inactivation and is separable from proteasomal degradation of E7, J. Virol. 75 (2001) 7583–7591.
[59] E. Berezutskaya, S. Bagchi, The human papillomavirus E7 oncoprotein functionally interacts with the S4 subunit of the 26 S proteasome, J. Biol. Chem. 272 (1997) 30135–30140.
[60] C.S. Hwang, A. Shemorry, A. Varshavsky, Two proteolytic pathways regulate DNA repair by cotargeting the Mgt1 alkylguanine transferase, Proc. Natl. Acad. Sci. U. S. A. 106 (2009) 2142–2147.
[61] K.F. Winklhofer, J. Tatzelt, C. Haass, The two faces of protein misfolding: gain- and loss-of-function in neurodegenerative diseases, EMBO J. 27 (2008) 336–349.
[62] J.S. Gibson, J.C. Ellory, Membrane transport in sickle cell disease, Blood Cells Mol. Dis. 28 (2002) 303–314.
[63] C.M. Dobson, Principles of protein folding, misfolding and aggregation, Semin. Cell Dev. Biol. 15 (2004) 3–16.
[64] E.K. Fredrickson, R.G. Gardner, Selective destruction of abnormal proteins by ubiquitin-mediated protein quality control degradation, Semin. Cell Dev. Biol. 23 (2012) 530–537.
[65] A. Luciani, V.R. Villella, S. Esposito, N. Brunetti-Pierri, D. Medina, C. Settembre, et al., Defective CFTR induces aggresome formation and lung inflammation in cystic fibrosis through ROS-mediated autophagy inhibition, Nat. Cell Biol. 12 (2010) 863–875.
[66] K. Du, P.H. Karp, C. Ackerley, J. Zabner, S. Keshavjee, E. Cutz, et al., Aggregates of mutant CFTR fragments in airway epithelial cells of CF lungs: new pathologic observations, J. Cyst. Fibros. 14 (2015) 182–193.
[67] C.L. Ward, S. Omura, R.R. Kopito, Degradation of Cftr by the ubiquitin-proteasome pathway, Cell 83 (1995) 121–127.
[68] P.J. Thomas, Y.H. Ko, P.L. Pedersen, Altered protein folding may be the molecular-basis of most cases of cystic-fibrosis, FEBS Lett. 312 (1992) 7–9.
[69] W.Q. Zhang, N. Fujii, A.P. Naren, Recent advances and new perspectives in targeting CFTR for therapy of cystic fibrosis and enterotoxin-induced secretory diarrheas, Future Med. Chem. 4 (2012) 329–345.
[70] Y. Park, S.K. Yoon, J.B. Yoon, The HECT domain of TRIP12 ubiquitinates substrates of the ubiquitin fusion degradation pathway, J. Biol. Chem. 284 (2009) 1540–1549.
[71] N. Hanoun, S. Fritsch, O. Gayet, V. Gigoux, P. Cordelier, N. Dusetti, et al., The E3 ubiquitin ligase thyroid hormone receptor-interacting protein 12 targets pancreas transcription factor 1a for proteasomal degradation, J. Biol. Chem. 289 (2014) 35593–35604.
[72] D. Larrieu, M. Brunet, C. Vargas, N. Hanoun, L. Ligat, L. Dagnon, et al., The E3 ubiquitin ligase TRIP12 participates in cell cycle progression and chromosome stability, Sci. Rep. 10 (2020).
[73] M. Kajiro, M. Tsuchiya, Y. Kawabe, R. Furumai, N. Iwasaki, Y. Hayashi, et al., The E3 ubiquitin ligase activity of Trip12 is essential for mouse embryogenesis, PLoS One 6 (2011).
[74] M. Knop, K. Siegers, G. Pereira, W. Zachariae, B. Winsor, K. Nasmyth, et al., Epitope tagging of yeast genes using a PCR-based strategy: more tags and improved practical routines, Yeast 15 (1999) 963–972.
[75] R.J. Baerends, K.N. Faber, A.M. Kram, J.A. Kiel, I.J. van der Klei, M. Veenhuis, A stretch of positively charged amino acids at the N terminus of Hansenula polymorpha Pex3p is involved in incorporation of the protein into the peroxisomal membrane, J. Biol. Chem. 275 (2000) 9986–9995.
[76] A. Khmelinskii, M. Meurer, N. Duishoev, N. Delhomme, M. Knop, Seamless gene tagging by endonuclease-driven homologous recombination, PLoS One 6 (2011) e23794.
[77] E.A. Winzeler, D.D. Shoemaker, A. Astromoff, H. Liang, K. Anderson, B. Andre, et al., Functional characterization of the S. cerevisiae genome by gene deletion and parallel analysis, Science 285 (1999) 901–906.
[78] Z. Li, F.J. Vizeacoumar, S. Bahr, J. Li, J. Warringer, F.S. Vizeacoumar, et al., Systematic exploration of essential yeast gene function with temperature-sensitive mutants, Nat. Biotechnol. 29 (2011) 361–367.

[79] A. Baryshnikova, M. Costanzo, S. Dixon, F.J. Vizeacoumar, C.L. Myers, B. Andrews, et al., Synthetic genetic array (SGA) analysis in Saccharomyces cerevisiae and Schizosaccharomyces pombe, Methods Enzymol. 470 (2010) 145–179.
[80] C.W. van Roermund, W.F. Visser, L. Ijlst, A. van Cruchten, M. Boek, W. Kulik, et al., The human peroxisomal ABC half transporter ALDP functions as a homodimer and accepts acyl-CoA esters, FASEB J. 22 (2008) 4201–4208.
[81] L.A. Gross, G.S. Baird, R.C. Hoffman, K.K. Baldridge, R.Y. Tsien, The structure of the chromophore within DsRed, a red fluorescent protein from coral, Proc. Natl. Acad. Sci. U. S. A. 97 (2000) 11990–11995.
[82] A. Khmelinskii, E. Blaszczak, M. Pantazopoulou, B. Fischer, D.J. Omnus, G. Le Dez, et al., Protein quality control at the inner nuclear membrane, Nature 516 (2014) 410–413.
[83] R. Saraya, M.N. Cepinska, J.A. Kiel, M. Veenhuis, I.J. van der Klei, A conserved function for Inp2 in peroxisome inheritance, Biochim. Biophys. Acta 1803 (2010) 617–622.
[84] A.M. Krikken, M. Veenhuis, I.J. van der Klei, Hansenula polymorpha pex11 cells are affected in peroxisome retention, FEBS J. 276 (2009) 1429–1439.
[85] S. Kumar, R. Singh, C.P. Williams, I.J. van der Klei, Stress exposure results in increased peroxisomal levels of yeast Pnc1 and Gpd1, which are imported via a piggybacking mechanism, Biochim. Biophys. Acta 1863 (2016) 148–156.